MID-AMERICA TRANSPORTATION CENTER

Report # MATC-UNL: 321

Final Report

Impact of Truck Loading on Design and Analysis of Asphaltic Pavement Structures-Phase II

Yong-Rak Kim, Ph.D.
Associate Professor
Department of Civil Engineering
University of Nebraska-Lincoln

Hoki Ban, Ph.D.
Soohyok Im, Ph.D. student

2011

A Cooperative Research Project sponsored by the U.S. Department of Transportation Research and Innovative Technology Administration

Impact of Truck Loading on Design and Analysis of Asphaltic Pavement Structures-Phase II

Hoki Ban, Ph.D.
Post-doctoral Research Associate
Department of Civil Engineering
University of Nebraska-Lincoln

Soohyok Im
Ph.D. Student
Department of Civil Engineering
University of Nebraska-Lincoln

Yong-Rak Kim, Ph.D.
Associate Professor
Department of Civil Engineering
University of Nebraska-Lincoln

A Report on Research Sponsored By

Mid-America Transportation Center

University of Nebraska-Lincoln

February 2011

Technical Report Documentation Page

1. Report No. 25-1121-0001-321	2. Government Accession No.	3. Recipient's Catalog No.
4. Title and Subtitle Impact of Truck Loading on Design and Analysis of Asphaltic Pavement Structures-Phase II		5. Report Date February 2011 6. Performing Organization Code
7. Author(s) Hoki Ban, Soohyok Im, and Yong-Rak Kim		8. Performing Organization Report No.
9. Performing Organization Name and Address		10. Work Unit No. (TRAIS) 11. Contract or Grant No.
12. Sponsoring Agency Name and Address Mid-America Transportation Center Region VII University Transportation Center University of Nebraska-Lincoln 2200 Vine Street, 262 Whittier Center P.O. Box 830851 Lincoln, Nebraska 68583-0851		13. Type of Report and Period Covered 14. Sponsoring Agency Code MATC TRB RiP No. 24489
15. Supplementary Notes		

16. Abstract

In this study, Schapery's nonlinear viscoelastic constitutive model is implemented into the commercial finite element (FE) software ABAQUS via user defined subroutine (user material, or UMAT) to analyze asphalt pavement subjected to heavy truck loads. Then, extensive creep-recovery tests are conducted at various stress levels and at two temperatures (30^{o}C and 40^{o}C) to obtain the stress- and temperature-dependent viscoelastic material properties of hot mix asphalt (HMA) mixtures. With the viscoelastic material properties characterized and the UMAT code, a typical pavement structure subjected to repeated heavy truck loads is modeled with the consideration of the effect of material nonlinearity with a realistic tire loading configuration. Three-dimensional finite element simulations of the pavement structure present significant differences between the linear viscoelastic approach and the nonlinear viscoelastic modeling in the prediction of pavement performance with respect to rutting and fatigue cracking. The differences between the two approaches are considered significant and should be addressed in the process of performance-based pavement design. This also implies the importance of proper and more realistic characterization of pavement materials.

17. Key Words	18. Distribution Statement		
19. Security Classif. (of this report) **Unclassified**	20. Security Classif. (of this page) **Unclassified**	21. No. of Pages **56**	22. Price

TABLE OF CONTENTS

LIST OF FIGURES

LIST OF TABLES

ACKNOWLEDGMENTS

The authors would like to thank the Mid-America Transportation Center (MATC) for their financial support needed to complete this study.

ABSTRACT

In this study, Schapery's nonlinear viscoelastic constitutive model is implemented into the commercial finite element (FE) software ABAQUS via user defined subroutine (user material, or UMAT) to analyze asphalt pavement subjected to heavy truck loads. Then, extensive creep-recovery tests are conducted at various stress levels and at two temperatures (30^{o}C and 40^{o}C) to obtain the stress- and temperature-dependent viscoelastic material properties of hot mix asphalt (HMA) mixtures. With the viscoelastic material properties characterized and the UMAT code, a typical pavement structure subjected to repeated heavy truck loads is modeled with the consideration of the effect of material nonlinearity with a realistic tire loading configuration. Three-dimensional finite element simulations of the pavement structure present significant differences between the linear viscoelastic approach and the nonlinear viscoelastic modeling in the prediction of pavement performance with respect to rutting and fatigue cracking. The differences between the two approaches are considered significant and should be addressed in the process of performance-based pavement design. This also implies the importance of proper and more realistic characterization of pavement materials.

CHAPTER 1 INTRODUCTION

Trucking is a key component of freight transportation in the US. Trucks moved 71% of the total tonnage and 80% of the total value of US shipments in 1998. By 2020, the US transportation system is expected to handle about 23 billion tons of cargo valued at nearly $30 trillion. More specifically, Table 1.1 presents information on freight shipments that have either an origin or a destination in Nebraska (FHWA Freight News 2002). As shown in the table, trucks moved a large percentage of the tonnage and value of shipments, and these values are expected to grow throughout the US over the next 10 years. Therefore, the need to preserve the existing highway infrastructure and to accomplish an appropriate design-analysis for new pavements is a high priority.

Table 1.1. Freight Shipments to, from, and within Nebraska (FHWA Freight News 2002)

	Tons (millions)			Value (billions $)		
Nebraska	**1998**	**2010**	**2020**	**1998**	**2010**	**2020**
Highway	155	212	250	93	169	261
Rail	46	59	69	8	13	19
Water	<1	<1	<1	<1	<1	<1
Air	<1	<1	<1	5	13	23

Roads are used to transport people and products from one point to another. From an economic perspective, travel time accounts for almost half of all costs experienced by highway users. The US has the largest network of roads of any country, with a total length of about 6.5 million kilometers; from this figure, 4.2 million kilometers are considered paved roads, of which 94% are asphalt surfaced.

An asphalt pavement is typically a multilayered system consisting of asphalt concrete, base, subbase, and subgrade layers. Multilayered elastic theory has been widely used for analysis

and design of flexible pavements. However, it is well-known that asphalt mixtures are viscoelastic; their stress and strain response is time-rate-temperature dependent. Therefore, the assumption of elasticity for an asphalt layer is misleading in predicting the performance of flexible pavements.

Recently, several studies (Al-Qadi et al. 2005; Elseifi et al. 2006; Kim et al. 2009) have conducted viscoelastic analyses that consider the asphalt layer as linear viscoelastic and the other layers as elastic, using the finite element (FE) method in two-dimensional (2-D) or three-dimensional (3-D) models for predicting the time-dependent response of flexible pavement. However, nonlinear response was not taken into consideration for their models in spite of abundant experimental observations (Collop et al. 2002; Masad and Somadevan 2002; Airey et al. 2004) that present nonlinear response of asphalt binders and mixes at certain levels of stress and strain. Therefore, it is necessary to consider the nonlinear viscoelastic responses when asphalt pavements are subjected to heavy truck loads.

To this end, Schapery's nonlinear viscoelastic model was employed to characterize the nonlinear viscoelastic behavior of asphalt mixtures. The model was implemented into the commercial FE software ABAQUS as a user-defined subroutine called UMAT (user material) based on the recursive-iterative numerical algorithm of Haji-Ali and Muliana (2004). Then, extensive creep-recovery tests were conducted at various stress levels and at two temperatures (30^{o}C and 40^{o}C) to obtain the stress- and temperature-dependent nonlinear viscoelastic material properties of hot mix asphalt (HMA) mixtures. Material properties were then used to simulate mechanical responses of pavement structures. Detailed investigations of the pavement responses resulting from different constitutive relations (such as linear viscoelastic and nonlinear

viscoelastic) can provide better understanding of the effects of truck loading on pavement damage and consequently advance the current pavement analysis-design method.

1.1 RESEARCH OBJECTIVES AND SCOPE

The primary objective of this study is to develop a mechanistic model for predicting pavement performance with particular focus on the impact of heavy truck loading on pavement damage. To meet this objective, a previous study (2009) investigated the effects of inelastic materials characterization (such as the viscoelastic nature of asphaltic materials) and the irregular pavement geometry (e.g., 3-D structure) on pavement responses, and this effort is continued in this research with an extended scope and more extensive details.

Specifically, we look at the impact of truck-loading configurations (realistic tire footprints) and the more realistic constitutive material behavior of the asphalt layer (nonlinear inelastic) in the prediction of pavement performance. Since the viscoelastic nature of asphaltic materials presents nonlinearity under high stress levels, the nonlinear viscoelastic response of asphaltic pavement subjected to heavy truck loads should be taken into account for more accurate predictions. Therefore, the specific objective of this study is to develop Schapery's nonlinear viscoelastic model and implement it into a commercial FE software via UMAT subroutine.

Any significant differences between analyses will be considered important factors that need to be treated with more care for better implementation of pavement analysis and design in the future.

1.2 ORGANIZATION OF THE REPORT

This report is composed of seven chapters. Following this introduction, Chapter 2 summarizes literature reviews for various constitutive models (such as linear elastic and linear

and nonlinear viscoelastic) and the FE analysis for flexible pavements. Chapter 3 presents the theoretical background of Schapery's nonlinear viscoelastic constitutive model and its numerical implementation into FE code. Verification of the nonlinear viscoelastic FE code is also presented in the chapter. In Chapter 4, the creep-recovery test conducted to identify linear and nonlinear viscoelastic material characteristics is described, and test results at different temperatures and stress levels are presented. Chapter 5 describes how the viscoelastic material properties are obtained from the creep-recovery test results of asphalt mixtures tested at different stress levels and temperatures. With the material properties identified from Chapter 5, Chapter 6 describes FE simulations of a pavement structure, taking into account the effect of material nonlinearity with a realistic tire loading configuration and structural geometry of the pavement. Simulation results with significant observations are then discussed in the chapter. Finally, the last chapter provides a summary and the conclusions for this study.

CHAPTER 2 LITERATURE REVIEW

Many researchers have made tremendous efforts to develop structural mechanistic models that are able to predict the performance of asphaltic pavements. In order to represent the behavior of asphalt mixtures under different traffic loads and climate conditions it is necessary to incorporate constitutive material models into these structural mechanistic models. In this chapter, various material models representing the mechanical response of asphalt mixtures for pavement analyses are described.

2.1 MULTILAYERED ELASTIC THEORY FOR FLEXIBLE PAVEMENTS

Burmister (1943) first developed solutions for a two-layered system and extended this work to a three-layer system with the assumption that each layer is homogenous, isotropic, and linearly elastic with an elastic modulus and Poisson's ratio. With the aid of a computer, the theory developed by Burmister can be applied to a multilayered system of any number of layers. Therefore, the multilayered elastic theory has been widely used for the structural analysis of flexible pavements.

As an example, the new pavement design guide, Mechanistic-Empirical Pavement Design Guide (MEPDG), has been developed and is currently under validation/implementation by many states. The MEPDG basically uses layered elastic theory to determine the mechanical responses in conjunction with empirically developed failure criteria called *transfer functions*. Although the MEPDG employs various design parameters (climate, traffic, materials, etc) to predict the performance of flexible pavements, it is known to be limited in its ability to accurately predict mechanical responses in asphaltic pavements. This limitation is due to the use of simplified structural analysis methods, a general lack of understanding of the fundamental constitutive

behavior and damage mechanisms for paving materials, and the use of circular tire loading configurations.

2.2 FINITE ELEMENT (FE) APPROACH FOR FLEXIBLE PAVEMENTS

The FE technique, in opposition to the MEPDG, has received increased attention from the pavement mechanics community due to its extremely versatile implementation of mechanical characteristics in addressing issues such as inelastic constitutive behavior, irregular pavement geometry (Helwany et al. 1998; Wang 2001; Blab and Harvey 2002; Al-Qadi et al. 2002, 2004, 2005), and growing damage (Collop et al. 2003; Mun et al. 2004; Kim et al. 2006). The following subsections provide various constitutive models for asphalt layer and loading configurations in the FE analyses.

2.2.1 Layer Elastic Modeling Approach of the Asphalt Layer

In order to determine an appropriate model for pavement analysis, Cho et al. (1996) analyzed flexible pavement under traffic loading using three different models: axisymmetric, 2-D plane strain, and 3-D. From linear elastic analysis, they found that axisymmetric and 3-D models yielded results comparable to those of layered elastic analyses, while the 2-D plane strain model produced overestimated responses.

Myers et al. (2001) attempted 2-D plane strain analysis instead of the axisymmetric model by incorporating a correction factor, which was defined as the tensile stress ratio of axisymmetric analysis to 2-D plane strain analysis. The results from 2-D plane strain analysis with the correction factor were comparable to the results from analysis of the axisymmetric model within the asphalt concrete surface layer.

Kim et al. (2005) investigated the effects of supersingle (wide-base) tire loadings on pavements using 2-D plane strain and 3-D static or dynamic analyses. They examined the

responses of pavement structure under two different subgrade materials, such as sand and clay. It was found that distresses from 2-D analysis were higher than those from 3-D analyses. It was also found that the permanent strain induced by supersingle tires was about four times greater than that of conventional tires.

The effects of loading configurations including axle type, axle load, and tire pressure at different vehicle speeds were investigated by Helwany et al. (1998) using FE analysis. It was reported that the axle load significantly influenced pavement responses, as was expected. A more interesting finding from the study is that only the radial strains and the longitudinal strains were affected by tire pressure for the axisymmetric analysis and the 3-D analysis, respectively.

The aforementioned FE studies assumed that asphalt layers are linear and elastic materials; however, asphalt materials are well-known viscoelastic materials that are significantly affected by rate of loadings and time as well as temperature. It has been observed that results from elastic analyses do not correlate well with field measurements. The mismatch between analysis results and field measurements is due to many factors, and one of the primary factors is strongly related to the elastic assumption, which is not suitable to characterize the time-rate-temperature dependent response of an asphalt layer in pavement. Therefore, many studies have considered the viscoelastic constitutive model for improvement in accuracy of the predicted behavior of asphalt materials, as presented in the following subsection.

2.2.2 Viscoelastic Modeling Approach of the Asphalt Layer

Kim et al. (2008) conducted 3-D linear viscoelastic modeling for asphalt concrete layers so as to evaluate the asphaltic pavement structure by comparing distresses from modeling with full-scale field test results. The results showed a good agreement.

A viscoelastic-plastic with growing damage model was used to investigate the permanent deformation of asphalt concrete by Zhao (2002). The model was developed from the theory of Schapery's continuum damage and work potential for elastic strain and viscoelastic components, while Uzan's strain hardening was used for the plastic strain component. Repetitive creep and recovery tests were performed at 40°C, which was high enough to allow accumulation of viscoplastic strain in the specimens. The viscoelastic-plastic model showed good predictions up to peak stress; however, it was not accurate beyond the peak of the stress-strain.

Another viscoelastic-plastic model was used by Al-Qablan et al. (2006) to simulate the asphalt pavement analyzer (APA), which enables measurement of the degree of rutting. The APA rutting depths for various types of asphalt mixtures were predicted, and it was concluded that the FE model showed very good agreement with the experimental results in simulating the APA rutting performance.

Yoo (2007) performed 3-D FE analysis in order to calculate creep strains after applying numerous heavy vehicular loading cycles by two different tire configurations (the dual tire assembly and the wide-base single tire assembly). Nonlinear time-hardening creep models, which were determined using repetitive creep and recovery tests in the laboratory, were used to characterize the creep behavior of hot-mix asphalt (HMA) at intermediate (20°C) and high (40°C) temperatures. It was found that the creep strain energy dissipation rate is different at the primary and secondary stages of loading time because the creep dissipation energy was ruled by the nonlinear time-hardening creep model. Therefore, a cumulative time-loading approach has been used in pavement analysis to consider a large number of loading repetitions in rutting analysis.

In addition to that method, several other studies (Elseifi et al. 2006; Al-Qadi et al. 2005; Yoo et al. 2006) have investigated the effect of loading configurations using the exact footprint shape and dimensions of tires with their actual wheel-axle configurations based on 3-D viscoelastic modeling methods. However, these studies used time steps to accurately simulate one pass of traffic loading, which may not be enough to identify the realistic time-dependent viscoelastic effects related to multiple load repetitions applied to pavements.

Recently, Huang et al (2011) developed a nonlinear viscoelastic-viscoplastic constitutive model and implemented it into a 3-D FE model of three-layer pavement structure to simulate the pavement response—the conclusion of which was pavement rutting performance. The study showed that FE simulations can successfully capture pavement responses under repeated loading at different temperatures.

CHAPTER 3 SCHAPERY'S NONLINEAR VISCOELASTICITY

In this chapter, a multiaxial nonlinear viscoelastic constitutive model developed by Schapery (1969) is briefly introduced, and the numerical implementation incorporated with the FE method is then described. Schapery's single integral constitutive model is implemented into the well-known commercial FE software ABAQUS via a user-defined material called UMAT. Following the model description, two example problems to verify the model and its numerical implementation are presented.

3.1 SCHAPERY'S NONLINEAR VISCOELASTIC MODEL

Schapery's nonlinear viscoelastic single-integral model for one-dimensional problems can be expressed in terms of an applied stress (σ^{τ}) as follows:

$$\varepsilon^t = \varepsilon(t) = g_0 D_0 \sigma^t + g_1 \int_0^t \Delta D\left(\psi^t - \psi^{\tau}\right) \frac{d\left(g_2 \sigma^{\tau}\right)}{d\tau} d\tau \tag{3.1}$$

where ψ is the reduced time given by:

$$\psi^t = \psi(t) = \int_0^t \frac{d\xi}{a_T a_\sigma} \tag{3.2}$$

where superscript t is current time; g_0, g_1, and g_2 are the nonlinear viscoelastic parameters related to stress status; a_T is the temperature shift factor; and a_σ is the stress shift factor. In addition to the temperature and stress effects, the effects for moisture and physical aging can also be included by adding their own time-scaling functions in Equation (3.2). The nonlinear effect considered in this study is only due to stress. These parameters are always positive and equal to one for the Boltzmann integral in linear viscoelasticity. D_0 is the instantaneous uniaxial elastic compliance, and ΔD is the uniaxial transient compliance. The uniaxial transient compliance can be expressed in the form of a Prony series as:

$$\Delta D^{\psi^t} = \sum_{n=1}^{N} D_n \left(1 - \exp\left(-\lambda_n \psi^t\right)\right) \tag{3.3}$$

where N is the number of terms, D_n is the *n*th coefficient of the Prony series, and λ_n is the *n*th reciprocal of retardation time.

Consequently, the shear transient compliance ΔJ^{ψ^t} and the bulk transient compliance ΔB^{ψ^t} can also be expressed by the Prony series as follows:

$$\Delta J^{\psi^t} = \sum_{n=1}^{N} J_n \left[1 - \exp\left(-\lambda_n t\right)\right] \tag{3.4}$$

$$\Delta B^{\psi^t} = \sum_{n=1}^{N} B_n \left[1 - \exp\left(-\lambda_n t\right)\right] \tag{3.5}$$

The one-dimensional integral in Equation (3.1) can be generalized to describe the multi-axial (e.g, 3-D) strain-stress relations for an isotropic media by decoupling the response into deviatoric and volumetric parts (Lai and Baker 1996) as follows:

$$e_{ij}^t = \frac{1}{2} g_0^t J_0 S_{ij}^t + \frac{1}{2} g_1^t \int_0^t \Delta J \left(\psi^t - \psi^\tau\right) \frac{d\left(g_2^\tau S_{ij}^\tau\right)}{d\tau} d\tau \tag{3.6}$$

$$\varepsilon_{kk}^t = \frac{1}{3} g_0^t B_0 \sigma_{kk}^t + \frac{1}{3} g_1^t \int_0^t \Delta B \left(\psi^t - \psi^\tau\right) \frac{d\left(g_2^\tau \sigma_{kk}^\tau\right)}{d\tau} d\tau \tag{3.7}$$

where J_0 and B_0 are the instantaneous elastic shear and bulk compliance, respectively.

Next, the nonlinear parameters are assumed to be general polynomial functions of the effective shear stress $\bar{\sigma}$ which can be written as:

$$g_0 = 1 + \sum_{i=1}^{n} \alpha_i \left\langle \frac{\bar{\sigma}}{\sigma_0} - 1 \right\rangle^i, \quad g_1 = 1 + \sum_{i=1}^{n} \beta_i \left\langle \frac{\bar{\sigma}}{\sigma_0} - 1 \right\rangle^i$$
$$g_2 = 1 + \sum_{i=1}^{n} \gamma_i \left\langle \frac{\bar{\sigma}}{\sigma_0} - 1 \right\rangle^i, \quad a_\sigma = 1 + \sum_{i=1}^{n} \delta_i \left\langle \frac{\bar{\sigma}}{\sigma_0} - 1 \right\rangle^i \tag{3.8}$$

where $\langle x \rangle = \begin{cases} x, & x > 0 \\ 0, & x \le 0 \end{cases}$, $\bar{\sigma} = \sqrt{\frac{3}{2} S_{ij} S_{ij}}$

The polynomial coefficients $(\alpha_i, \beta_i, \gamma_i, \delta_i)$ can be calibrated from the creep and recovery tests. The term σ_0 is the effective shear stress limit that determines the end of the linear viscoelastic range. It is further assumed that Poisson's ratio υ is time-independent. This allows use of the same nonlinear and transient parameters for the 3-D problems in a single integral relation as:

$$\begin{aligned} \varepsilon_{ij}^t &= e_{ij}^t + \frac{1}{3} \varepsilon_{kk}^t \delta_{ij} \\ &= (1+\upsilon) D_0 g_0 S_{ij}^t + (1+\upsilon) g_1 \int_0^t \Delta D\left(\psi^t - \psi^\tau\right) \frac{d\left(g_2 S_{ij}^\tau\right)}{d\tau} d\tau \\ &= \frac{(1-2\upsilon)}{3} \delta_{ij} \left[D_0 g_0 \sigma_{kk} + g_1 \int_0^t \Delta D\left(\psi^t - \psi^\tau\right) \frac{d\left(g_2 \sigma_{kk}^\tau\right)}{d\tau} d\tau \right] \end{aligned} \tag{3.9}$$

Comparing the terms in Equation (3.6) and (3.7) with those in Equation (3.9) yields:

$$\begin{aligned} &J_0 = 2(1+\upsilon) D_0 \qquad B_0 = 3(1-2\upsilon) D_0 \\ &\Delta J(\psi) = 2(1+\upsilon) \Delta D(\psi) \qquad \Delta B(\psi) = 3(1-2\upsilon) \Delta D(\psi) \end{aligned} \tag{3.10}$$

Next, the deviatoric and volumetric components can be expressed in terms of the hereditary integral formulation by substituting Equation (3.4) into (3.6) and (3.5) into (3.7) as follows (Haj-Ali and Muliana 2004).

$$e_{ij}^t = \frac{1}{2} \left[g_0^t J_0 + g_1^t g_2^t \sum_{n=1}^{N} J_n \right] S_{ij}^t - \sum_{n=1}^{N} q_{ij,n}^t \tag{3.11}$$

$$\varepsilon_{kk}^{t} = \frac{1}{3}\left[g_0^t B_0 + g_1^t g_2^t \sum_{n=1}^{N} B_n \right] \sigma_{kk}^{t} - \sum_{n=1}^{N} q_{kk,n}^{t} \tag{3.12}$$

where

$$q_{ij,n}^{t} = \frac{1}{2} g_1 \int_0^t J_n \exp\left[-\lambda_n \left(\psi^t - \psi^\tau \right) \right] \frac{d\left(g_2 S_{ij} \right)}{d\tau} d\tau \tag{3.13}$$

$$q_{kk,n}^{t} = \frac{1}{3} g_1 \int_0^t B_n \exp\left[-\lambda_n \left(\psi^t - \psi^\tau \right) \right] \frac{d\left(g_2 \sigma_{kk} \right)}{d\tau} d\tau \tag{3.14}$$

3.2 NUMERICAL IMPLEMENTATION

As can be seen in equations from the previous sub-section, the nonlinear viscoelastic constitution is expressed as a time- and history-dependent integral. In order to include the viscoelastic constitution into a numerical code, it may be incrementalized so that history dependence is retained at each time step. Considering incremental time step Δt, the integral expression of Equation (3.13) can be rewritten as:

$$\begin{aligned} q_{ij,n}^{t} = & \frac{1}{2} g_1 \int_0^{t-\Delta t} J_n \exp\left[-\lambda_n \left(\psi^t - \psi^\tau \right) \right] \frac{d\left(g_2 S_{ij} \right)}{d\tau} d\tau \\ & + \frac{1}{2} g_1 \int_{t-\Delta t}^{t} J_n \exp\left[-\lambda_n \left(\psi^t - \psi^\tau \right) \right] \frac{d\left(g_2 S_{ij} \right)}{d\tau} d\tau \end{aligned} \tag{3.15}$$

The incremental reduced time is defined by:

$$\Delta\psi^t = \psi^t - \psi^{t-\Delta t} \tag{3.16}$$

since

$$\exp\left[-\lambda_n \left(\psi^t - \psi^\tau \right) \right] = \exp\left[-\lambda_n \left(\psi^t - \Delta\psi^t - \psi^\tau \right) \right] \cdot \exp\left[-\lambda_n \Delta\psi^t \right] \tag{3.17}$$

The first integral in Equation (3.15) can be rewritten as:

$$\int_0^{t-\Delta t} J_n \exp\left[-\lambda_n\left(\psi^t-\psi^\tau\right)\right]\frac{d\left(g_2 S_{ij}\right)}{d\tau}d\tau$$
$$= \exp\left[-\lambda_n \Delta\psi^t\right]\int_0^{t-\Delta t} J_n \exp\left[-\lambda_n\left(\psi^t-\Delta\psi^t-\psi^\tau\right)\right]\frac{d\left(g_2 S_{ij}\right)}{d\tau}d\tau \tag{3.18}$$

The second integral of Equation (3.15) is carried out by parts while assuming that shift parameters are constant and S_{ij} varies linearly over the current time increment Δt. Therefore, the second integral can be evaluated:

$$\int_{t-\Delta t}^{t} J_n \exp\left[-\lambda_n\left(\psi^t-\psi^\tau\right)\right]\frac{d\left(g_2 S_{ij}\right)}{d\tau}d\tau = \frac{1-\exp\left[-\lambda_n\Delta\psi^t\right]}{\lambda_n\Delta\psi^t}\left(g_2^t S_{ij}^t - g_2^{t-\Delta t} S_{ij}^{t-\Delta t}\right) \tag{3.19}$$

Substituting Equations (3.18) and (3.19) into Equation (3.15) yields:

$$q_{ij,n}^t = \frac{1}{2} g_1 J_n \left[\exp\left[-\lambda_n\Delta\psi^t\right] q_{ij,n}^{t-\Delta t} + \frac{1-\exp\left[-\lambda_n\Delta\psi^t\right]}{\lambda_n\Delta\psi^t}\left(g_2^t S_{ij}^t - g_2^{t-\Delta t} S_{ij}^{t-\Delta t}\right)\right] \tag{3.20}$$

Similarly, the following recursive expression for $q_{kk,n}^t$ in Equation (3.15) can be derived:

$$q_{kk,n}^t = \frac{1}{3} g_1 B_n \left[\exp\left[-\lambda_n\Delta\psi^t\right] q_{kk,n}^{t-\Delta t} + \frac{1-\exp\left[-\lambda_n\Delta\psi^t\right]}{\lambda_n\Delta\psi^t}\left(g_2^t \sigma_{kk}^t - g_2^{t-\Delta t} \sigma_{kk}^{t-\Delta t}\right)\right] \tag{3.21}$$

The terms $q_{ij,n}^{t-\Delta t}$ and $q_{kk,n}^{t-\Delta t}$ are the shear and volumetric hereditary integrals for every term in the Prony series expressed at the end of previous time increment $\left(t-\Delta t\right)$. Therefore, deviatoric strain and volumetric strain can be obtained by substituting Equation (3.20) into (3.11) and (3.21) into (3.12). Resulting expressions are presented as follows:

$$
\begin{aligned}
e_{ij}^{t} &= \frac{1}{2}\left[g_0^t J_0 + g_1^t g_2^t \sum_{n=1}^{N} J_n - g_1^t g_2^t \sum_{n=1}^{N} J_n \frac{1-\exp\left[-\lambda_n \Delta\psi^{t}\right]}{\lambda_n \Delta\psi^{t}} \right] S_{ij}^{t} \\
&\quad -\frac{1}{2} g_1^t \sum_{n=1}^{N} J_n \left[\exp\left[-\lambda_n \Delta\psi^{t}\right] q_{ij,n}^{t-\Delta t} - g_2^{t-\Delta t} \frac{1-\exp\left[-\lambda_n \Delta\psi^{t}\right]}{\lambda_n \Delta\psi^{t}} S_{ij}^{t-\Delta t} \right] \\
&= J^{*} S_{ij}^{t} - d_{ij}^{t}
\end{aligned}
\tag{3.22}
$$

$$
\begin{aligned}
\varepsilon_{kk}^{t} &= \frac{1}{3}\left[g_0^t B_0 + g_1^t g_2^t \sum_{n=1}^{N} B_n - g_1^t g_2^t \sum_{n=1}^{N} B_n \frac{1-\exp\left[-\lambda_n \Delta\psi^{t}\right]}{\lambda_n \Delta\psi^{t}} \right] \sigma_{ij}^{t} \\
&\quad -\frac{1}{3} g_1^t \sum_{n=1}^{N} B_n \left[\exp\left[-\lambda_n \Delta\psi^{t}\right] q_{kk,n}^{t-\Delta t} - g_2^{t-\Delta t} \frac{1-\exp\left[-\lambda_n \Delta\psi^{t}\right]}{\lambda_n \Delta\psi^{t}} \sigma_{ij}^{t-\Delta t} \right] \\
&= B^{*} \sigma_{kk}^{t} - V_{kk}^{t}
\end{aligned}
\tag{3.23}
$$

Next, in order to be implemented in the FE method, the incremental deviatoric and bulk strains are derived and expressed as:

$$
\begin{aligned}
\Delta e_{ij}^{t} &= e_{ij}^{t} - e_{ij}^{t-\Delta t} \\
&= J^{*t} S_{ij}^{t} - J^{*t-\Delta t} S_{ij}^{t-\Delta t} - \frac{1}{2} \sum_{n=1}^{N} J_n \left(g_1^t \exp\left[-\lambda_n \Delta\psi^{t}\right] - g_1^{t-\Delta t} \right) q_{ij,n}^{t-\Delta t} \\
&\quad -\frac{1}{2} g_2^{t-\Delta t} \sum_{n=1}^{N} J_n \left[g_1^{t-\Delta t} \left(\frac{1-\exp\left[-\lambda_n \Delta\psi^{t-\Delta t}\right]}{\lambda_n \Delta\psi^{t-\Delta t}} \right) - g_1^t \left(\frac{1-\exp\left[-\lambda_n \Delta\psi^{t}\right]}{\lambda_n \Delta\psi^{t}} \right) \right] S_{ij}^{t-\Delta t}
\end{aligned}
\tag{3.24}
$$

$$
\begin{aligned}
\Delta \varepsilon_{kk}^{t} &= \varepsilon_{kk}^{t} - \varepsilon_{kk}^{t-\Delta t} \\
&= B^{*t} \sigma_{kk}^{t} - B^{*t-\Delta t} \sigma_{kk}^{t-\Delta t} - \frac{1}{3} \sum_{n=1}^{N} B_n \left(g_1^t \exp\left[-\lambda_n \Delta\psi^{t}\right] - g_1^{t-\Delta t} \right) q_{kk,n}^{t-\Delta t} \\
&\quad -\frac{1}{3} g_2^{t-\Delta t} \sum_{n=1}^{N} B_n \left[g_1^{t-\Delta t} \left(\frac{1-\exp\left[-\lambda_n \Delta\psi^{t-\Delta t}\right]}{\lambda_n \Delta\psi^{t-\Delta t}} \right) - g_1^t \left(\frac{1-\exp\left[-\lambda_n \Delta\psi^{t}\right]}{\lambda_n \Delta\psi^{t}} \right) \right] \sigma_{ij}^{t-\Delta t}
\end{aligned}
\tag{3.25}
$$

Although Equations (3.24) and (3.25) can be used to determine the unknown stress increment for a given strain increment, stress-dependent nonlinear parameters are still unknown

at the current time. Therefore, an iterative calculation is necessary to find the correct stress states. To do this, Equations (3.24) and (3.25) are further linearized using the following approximations:

$$\begin{aligned} g_s^t &= g_s^{t-\Delta t}, \quad s = 0,1,2 \\ \Delta\psi^t &= \Delta\psi^{t-\Delta t} \end{aligned} \tag{3.26}$$

Then, the trial incremental stresses can be expressed as:

$$\Delta S_{ij}^{t,tr} = \frac{1}{J^{*t,tr}} \left[\Delta e_{ij}^t + \frac{1}{2} g_1^{t,tr} \sum_{n=1}^{N} J_n \left(\exp\left[-\lambda_n \Delta\psi^t \right] - 1 \right) q_{ij,n}^{t-\Delta t} \right] \tag{3.27}$$

$$\Delta \sigma_{kk}^{t,tr} = \frac{1}{B^{*t,tr}} \left[\Delta e_{ij}^t + \frac{1}{3} g_1^{t,tr} \sum_{n=1}^{N} B_n \left(\exp\left[-\lambda_n \Delta\psi^t \right] - 1 \right) q_{ij,n}^{t-\Delta t} \right] \tag{3.28}$$

In this study, an iterative scheme is employed to obtain the correct stress state for a given strain increment. The iterative scheme is developed by defining strain residuals R_{ij}. The residuals can be defined by using incremental strains in Equations (3.24) and (3.25) as follows:

$$R_{ij}^t = \Delta e_{ij}^t + \frac{1}{3} \Delta \varepsilon_{kk}^t - \Delta \varepsilon_{ij}^t \tag{3.29}$$

A Jacobian matrix is then determined by taking the derivative of the residual vector with respect to the incremental stress vector in order to minimize the strain residuals. The following expression is used to form the Jacobian matrix.

$$
\begin{aligned}
\frac{\partial R_{ij}^{t}}{\partial \sigma_{kl}^{t}} &= J^{*t}\delta_{ik}\delta_{jl} + \frac{1}{3}\left(B^{*t} - J^{*t}\right)\delta_{ij}\delta_{kl} \\
&+ \frac{\partial \bar{\sigma}^{t}}{\partial \sigma_{kl}^{t}}\left\{ \frac{\partial J^{*}}{\partial \Delta\bar{\sigma}^{t}}\sigma_{ij}^{t} + \frac{1}{3}\left(\frac{\partial B^{*t}}{\partial \Delta\bar{\sigma}^{t}} - \frac{\partial J^{*}}{\partial \Delta\bar{\sigma}^{t}} \right)\sigma_{kk}^{t}\delta_{ij} \right. \\
&- \frac{1}{2}\frac{\partial g_1^{t}}{\partial \bar{\sigma}^{t}} \sum_{n=1}^{N} J_n \left[\exp\left[-\lambda_n \Delta\psi^{t}\right] q_{ij,n}^{t-\Delta t} - g_2^{t-\Delta t}\left(\frac{1-\exp\left[-\lambda_n \Delta\psi^{t}\right]}{-\lambda_n \Delta\psi^{t}} \right) S_{ij}^{t-\Delta t} \right] \\
&- \frac{1}{2}\frac{\partial a_{\sigma}^{t}}{\partial \bar{\sigma}^{t}} \sum_{n=1}^{N} J_n \left[\exp\left[-\lambda_n \Delta\psi^{t}\right]\left(\frac{\lambda_n \Delta t q_{ij,n}^{t-\Delta t}}{\left(a_{\sigma}^{t}\right)^2} + \frac{S_{ij}^{t-\Delta t}}{\left(a_{\sigma}^{t}\right)} \right) \right. \\
&\left. - g_2^{t-\Delta t}\left(\frac{1-\exp\left[-\lambda_n \Delta\psi^{t}\right]}{-\lambda_n \Delta\psi^{t}} \right) S_{ij}^{t-\Delta t} \right] \\
&- \frac{1}{9}\frac{\partial g_1^{t}}{\partial \bar{\sigma}^{t}} \sum_{n=1}^{N} B_n \left[\exp\left[-\lambda_n \Delta\psi^{t}\right] q_{kk,n}^{t-\Delta t} - g_2^{t-\Delta t}\left(\frac{1-\exp\left[-\lambda_n \Delta\psi^{t}\right]}{-\lambda_n \Delta\psi^{t}} \right) \sigma_{kk}^{t-\Delta t} \right] \delta_{ij} \\
&- \frac{1}{9}\frac{\partial a_{\sigma}^{t}}{\partial \bar{\sigma}^{t}} \sum_{n=1}^{N} B_n \left[\exp\left[-\lambda_n \Delta\psi^{t}\right]\left(\frac{\lambda_n \Delta t q_{kk,n}^{t-\Delta t}}{\left(a_{\sigma}^{t}\right)^2} + \frac{\sigma_{kk}^{t-\Delta t}}{\left(a_{\sigma}^{t}\right)} \right) \right. \\
&\left. \left. - g_2^{t-\Delta t}\left(\frac{1-\exp\left[-\lambda_n \Delta\psi^{t}\right]}{-\lambda_n \Delta\psi^{t}} \right) \sigma_{kk}^{t-\Delta t} \right] \delta_{ij} \right\}
\end{aligned}
\tag{3.30}
$$

where $\dfrac{\partial \bar{\sigma}^{t}}{\partial \sigma_{kl}^{t}} = \dfrac{3}{2}\dfrac{S_{ij}^{t}}{\Delta\bar{\sigma}^{t}}\left(\delta_{ij}\delta_{jl} - \dfrac{1}{3}\delta_{ij}\delta_{kl} \right)$

Finally, a consistent tangent compliance is defined by taking the partial derivative of the incremental strain with respect to the incremental stress at the end of the current time step. Using Equation (3.29), the consistent tangent compliance matrix C_{ijkl}^{t} at the converged state is as follows:

$$
C_{ijkl}^{t} = \frac{\partial \Delta\varepsilon_{ij}^{t}}{\Delta\sigma_{kl}^{t}} = \frac{\partial R_{ij}^{t}}{\partial \Delta\sigma_{kl}^{t}} \tag{3.31}
$$

3.3 MODEL VERIFICATION

The UMAT subroutine code developed in this study can be verified by simply comparing computational results from FE simulations with analytical results obtained from simple problems. The problems to be analyzed for verifying the code are shown in Figure 3.1.

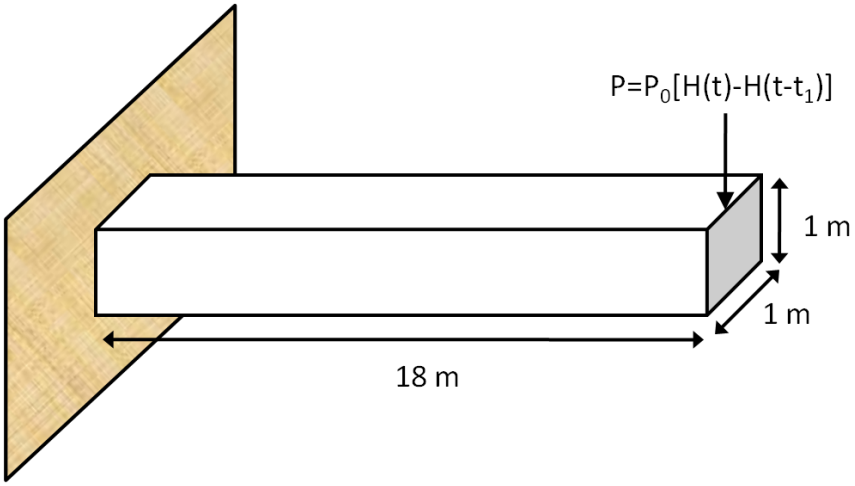

(a) cantilever beam with a tip load

$$\sigma(t) = \sigma_a H(t) - (\sigma_a - \sigma_b) H(t - t_a)$$

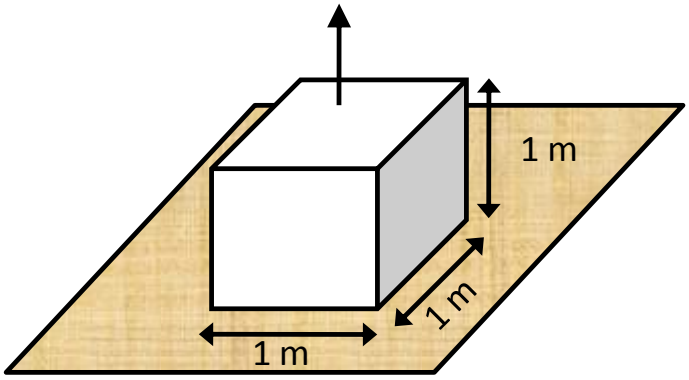

(a) uniaxial bar in tension

Figure 3.1. Example Problems to Verify the UMAT Code

3.3.1 Example No.1 (Cantilever Beam with Tip Load)

Consider the cantilever beam shown in Figure 3.1(a). The beam has a length L of 18 m and a cross-sectional area in square $A = 1m^2$.

As shown, the cantilever beam is subjected to a transient concentrated tip load:

$$P = P_0\left[H(t) - H(t - t_1)\right] \tag{3.32}$$

where $P_0 = 1\text{N}$, t_1=10 sec, and H is the Heaviside step function.

Suppose the cantilever beam is a linear viscoelastic material. Its analytical solution for tip displacements can be obtained by applying the standard viscoelastic correspondence principle to elastic solution as follows:

$$\delta_{tip} = \frac{P_0 L^3}{3I}\left[D(t) - D(t - t_1)H(t - t_1)\right] \tag{3.33}$$

where I is the area moment of inertia of the cross-section (in this case 1/12 m^4) and the creep compliance $D(t)$ is given by

$$D(t) = D_0 + D_1\left(1 - \exp\left[-\lambda t\right]\right) \tag{3.34}$$

where $D_0 \equiv \frac{1}{E_0}, E_0 \equiv E_\infty + E_1, D_1 \equiv \frac{1}{E_\infty} - \frac{1}{E_0}, \lambda = \frac{E_\infty}{E_0} \cdot \frac{1}{\rho}$

Linear viscoelastic material properties for the Prony series are necessary for the code verification. Relatively simple and arbitrarily determined linear viscoelastic stress relaxation moduli (E values) and a relaxation time (ρ) were used, since this problem is merely for code verification. Modulus values, E_1 of 0.4MPa, E_∞ of 0.1 MPa, and the relaxation time (ρ value) of 1.0 sec were used.

For the UMAT code verification, a special case of nonlinear viscoelastic response where $g_0 = g_1 = g_2 = a_\sigma = 1$ was simulated. When the nonlinear viscoelastic model parameters are all equal to unity, the nonlinear viscoelastic model reduces to a linear viscoelastic hereditary integral. An analytical linear viscoelastic solution can then be calculated and compared to the computational results from the FE analysis. Good agreement between the two results infers that the code was developed appropriately. However, it should be noted that a strength of the materials solution—the analytical solution as shown in Equation (3.33)—is not exact, but is considered a good approximation for a beam with ratio of 18:1, which is the case for this example problem. As shown in Figure 3.2, the linear viscoelastic FE prediction and analytical solution match very well.

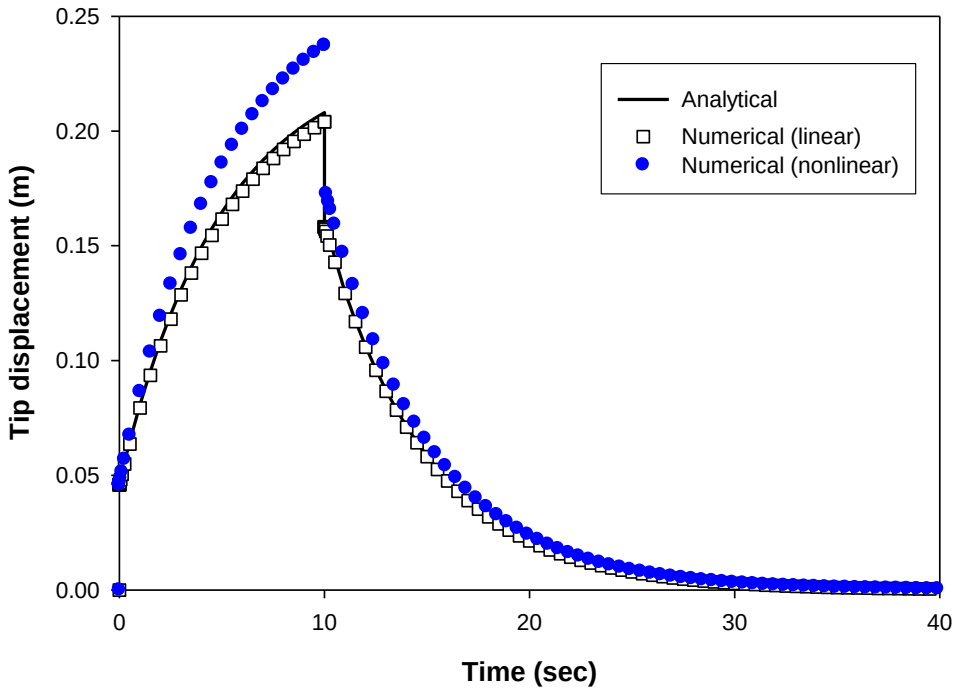

Figure 3.2. Model Verification Example: Cantilever Beam with Tip Load

Secondly, in an attempt to check the role of material nonlinearity in the model, the same beam problem was simulated by assuming that the two parameters (g_0 and a_σ) are equal to unity, while the other two nonlinear parameters (g_1 and g_2) are linear functions of effective shear stress as follows:

$$g_1 = 1 + 0.005\left(\frac{\bar{\sigma}}{\sigma_0} - 1\right)$$
$$g_2 = 1 + 0.005\left(\frac{\bar{\sigma}}{\sigma_0} - 1\right) \tag{3.35}$$

Tip displacements in circular dots are plotted in Figure 3.2. As presented in the figure, instantaneous strains resulting from the linear viscoelastic analytical solution and the FE simulations with linear and nonlinear viscoelastic models are all identical, but later strains from the nonlinear viscoelastic simulation are greater than those for the other linear viscoelastic cases. This seems reasonable because the nonlinear parameter g_0, which contributes to instantaneous response, is set at one whereas the other parameters that affect later-stage mechanical responses are represented by functions, as shown in Equation (3.35).

3.3.2 Example No. 2 (Uniaxial Bar in Two-Step Tensile Loading)

The second example problem to verify the UMAT code is a simple nonlinear viscoelastic uniaxial bar subjected to a two-step tensile load as presented in Figure 3.3. The first loading of 1N is applied for 10 sec and then reduced to 0.5N for 40 sec. The resulting strain response can be derived as:

$$\varepsilon_c = \left[g_0^a D_0 + g_1^a g_2^a \Delta D\left(\frac{t}{a_\sigma^a}\right)\right]\sigma_a \qquad \text{for } 0 < t < t_a \tag{3.36}$$

$$\varepsilon_r = g_0^b D_0 \sigma_b + g_1^b \left[g_2^a \sigma_a \Delta D\left(\frac{t_a}{a_\sigma^a} + \frac{t - t_a}{a_\sigma^b} \right) + \left(g_2^b \sigma_b - g_2^a \sigma_a \right) \Delta D\left(\frac{t - t_a}{a_\sigma^b} \right) \right] \quad \text{for } t_a < t < t_b \quad (3.37)$$

where $\Delta D(t) = D_1(1 - \exp(-\lambda t))$, $t_a = 10$, and $t_b = 40\,\text{sec}$.

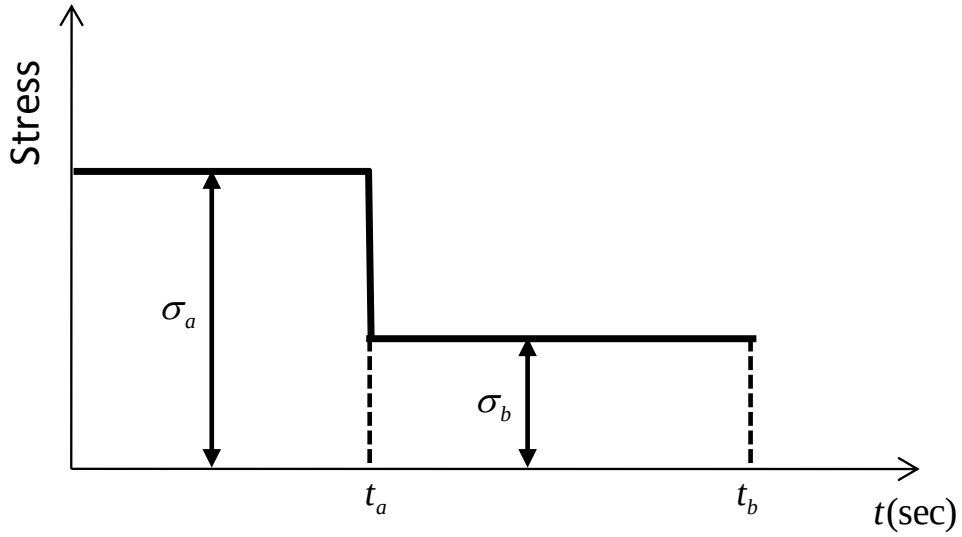

Figure 3.3. Two-Step Loading Sequence

For simplicity, all nonlinear viscoelastic material parameters during the first loading stage are assumed as $g_0^a = g_1^a = g_2^a = a_\sigma^a = 1.1$ and returned to unity when the second loading is applied. As demonstrated in Figure 3.4, FE simulation results show a good agreement with analytical solutions calculated using Equations (3.36) and (3.37). This further confirms that the UMAT code has been developed appropriately and can be used to simulate nonlinear viscoelastic responses of general structures (such as pavements) that present complicated geometry and boundary conditions.

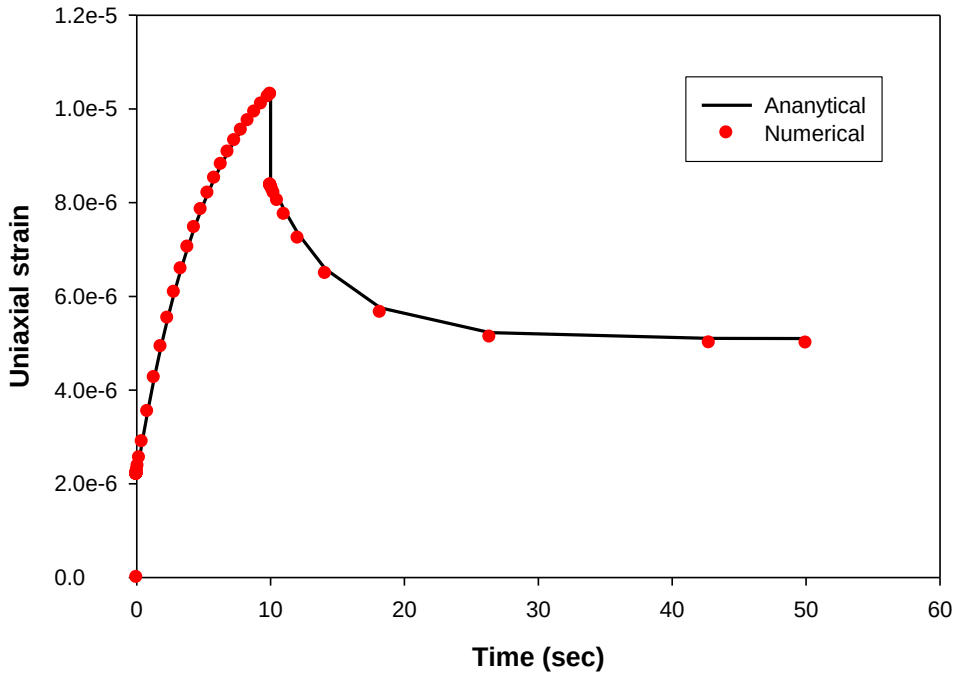

Figure 3.4. Model Verification Example: Uniaxial Bar with Two-Step Loading

CHAPTER 4 MATERIALS AND LABORATORY TESTS

This chapter briefly describes materials used and laboratory tests performed in this study. Two different asphalt mixtures were selected to conduct creep-recovery tests at varying stress levels and different temperatures. Test results are used to identify linear and nonlinear viscoelastic material properties of the mixtures, which are described in the next chapter.

4.1 MATERIALS

Table 4.1 summarizes mixture information including Superpave PG asphalt binder grade, aggregates in each mixture, and gradation resulting from combined blend of aggregates. As shown in the table, each mixture was designed through the blending of different mixture components. The two asphalt concrete mixtures were produced in order to achieve the 4% ± 1% air voids required for Superpave methodology; for that reason, different percentages of binder content were necessary for each mixture. Binder contents, 6.00% and 5.60%, were determined as appropriate values that satisfy all key volumetric characteristics of asphalt mixtures.

Table 4.1. Mixture Information

Mixture ID	Binder PG	Aggregate Gradation (% Passing on Each Sieve)									% Binder	% Voids
		19mm	12.5mm	9.5mm	#4	#8	#16	#30	#50	#200		
1	64-28	100	95	89	72	36	21	14	10	3.5	6.00	4.09
2	70-28	100	97	91.2	80.5	55.8	37.4	23.2	14.5	5.4	5.60	3.68

4.2 SPECIMEN FABRICATION

To conduct the uniaxial static creep-recovery tests, a Superpave gyratory compactor was used to produce the cylindrical samples with a diameter of 150 mm and an approximate height of 170 mm. Then, the compacted samples were cored and sawn to produce testing specimens targeting an air void of 4% ± 0.5% with a 100-mm diameter and 150-mm height. Figure 4.1 presents a specimen after the compaction and coring-sawing process.

Figure 4.1. A Specimen Cored and Sawn from the Gyratory Compacted Sample

To measure the axial displacement of the specimen under the static compressive force, epoxy glue was used to fix mounting studs to the surface of the specimen so that the three linear variable differential transformers (LVDTs) could be attached onto the surface of the specimen at 120^{o} radial intervals with a 100-mm gauge length, as illustrated in Figure 4.2. Then, the specimen was mounted in the UTM-25kN testing station for creep-recovery testing (Figure 4.3).

Figure 4.2. A Device Used to Place the Mounting Studs for LVDTs

Figure 4.3. A Specimen with LVDTs Mounted in the UTM-25kN

4.3 CREEP-RECOVERY TEST

The static creep-recovery test was conducted on replicate specimens of each asphalt mixture at two different temperatures: 30^{o}C for Mixture 1 and 40^{o}C for Mixture 2. A creep stress for 30 seconds (followed by recovery for 1,000 seconds) was applied to the specimens, and the vertical deformation (in compression) was monitored with the three LVDTs. Various stress levels were applied to characterize nonlinear behavior of asphalt mixtures for a large range of stress levels.

Table 4.2 presents applied stress levels and the testing temperature for each mixture. Based on the preliminary test results, the threshold stress (reference stress) of nonlinear viscoelasticity was found to be 700 kPa at 30^{o}C (Mixture 1) and 400 kPa at 40^{o}C (Mixture 2). In other words, the asphalt mixtures are considered linear viscoelastic below the reference stress level at that testing temperature. Figure 4.4 presents test results. As expected, the higher stress level generated larger creep strain and recovered less strain for both testing temperatures.

Table 4.2. Applied Stress Levels for Each Mixture

Mix	Temp.	Stress Level (kPa)					
Mixture 1	30°C	700	1,000	1,200	1,500		
Mixture 2	40°C	400	600	800	1,000	1,200	1,500

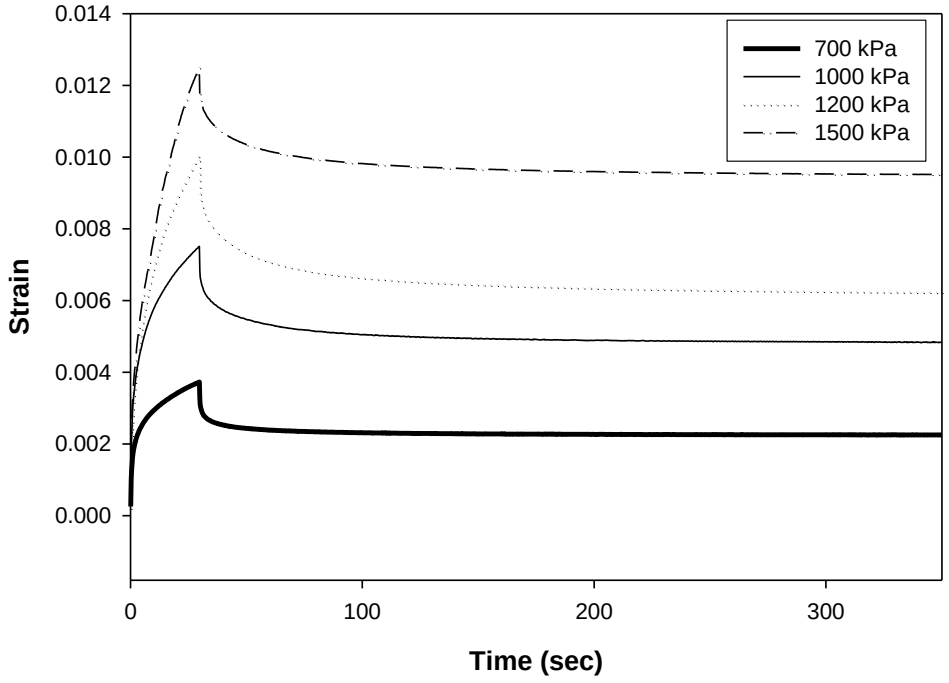

(a) Mixture 1 at 30^{o}C

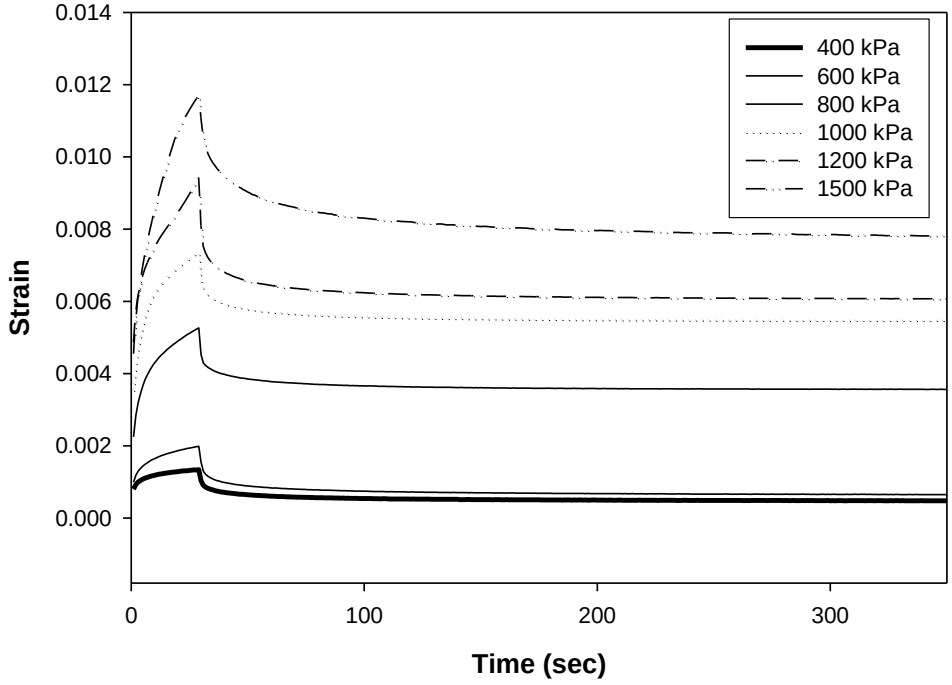

(b) Mixture 2 at 40^{o}C

Figure 4.4. Creep-Recovery Test Results at Various Stress Levels

CHAPTER 5 CHARACTERIZATION OF VISCOELASTIC PROPERTIES

In this chapter, the creep-recovery test results presented in the previous chapter are used to identify viscoelastic material properties. As presented in the following subsection, the procedure to define nonlinear viscoelastic properties started from the identification of linear viscoelastic material properties using the test results at the threshold stress level. The linear viscoelastic properties were then used to find nonlinear viscoelastic properties by using creep-recovery test data resulting from higher stress levels than the threshold level. After all viscoelastic material properties (linear and nonlinear) were found, model validation was pursued by comparing model simulations with experimental test results. Results are presented in this chapter.

5.1 VISCOELASTIC MATERIAL PROPERTIES

A schematic of a single creep-recovery test is illustrated in Figure 5.1 for a constant stress loading and unloading condition. For loading time period, i.e., $0 < t < t_1$, Equation (3.1) can be expressed as:

$$\varepsilon_c(t) = g_0 D_0 \sigma + g_1 g_2 \sigma \Delta D\left(\frac{t}{a_\sigma}\right) \tag{5.1}$$

For unloading time period, that is, $t > t_1$, it can be expressed as:

$$\varepsilon_r(t) = g_2 \sigma\left[\Delta D\left(\frac{t_1}{a_\sigma} + t - t_1\right) - \Delta D\left(t - t_1\right)\right] \tag{5.2}$$

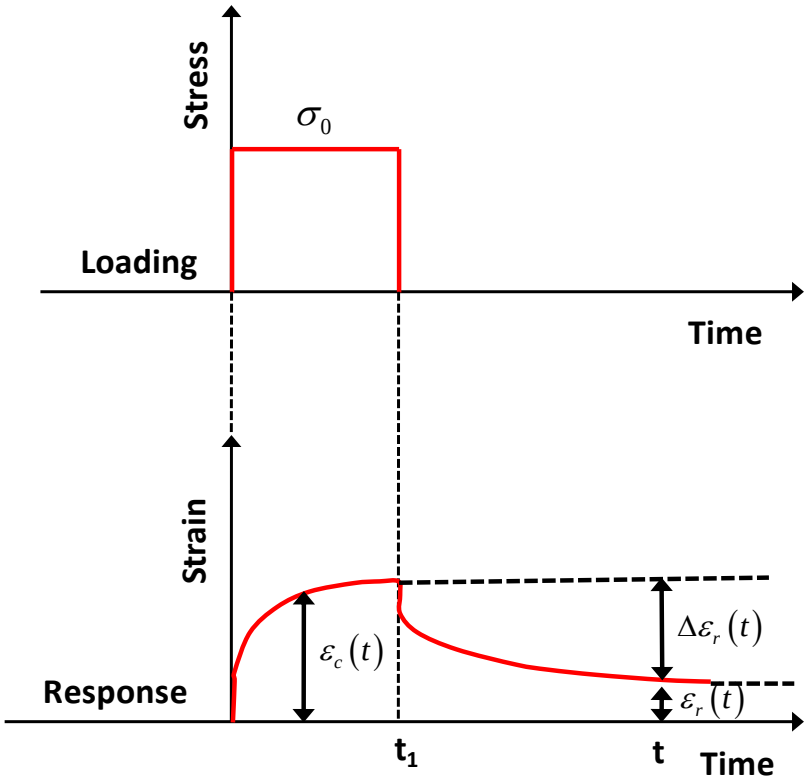

Figure 5.1. A Schematic of a Single Creep-Recovery Test

The first step is to obtain the Prony series coefficients in Equation (3.3) from linear viscoelastic response at the threshold stress level of each considered temperature. Since the recoverable response is linear viscoelastic ($g_0 = g_1 = g_2 = a_\sigma = 1$) at the threshold stress level, the recovered strain $\Delta\varepsilon_r$ shown in Figure 5.1 can be used to obtain the linear viscoelastic Prony series coefficients. Substituting Equation (3.3) into Equations (5.1) and (5.2) yields:

$$\begin{aligned}\Delta\varepsilon_r &= \varepsilon_c(t_1) - \varepsilon_r(t) \\ &= \sigma\left\{\begin{array}{l}\displaystyle\sum_{n=1}^{N} D_n\left[1-\exp\left(-\lambda_n t_1\right)\right] - \\ \displaystyle\sum_{n=1}^{N} D_n\left[1-\exp\left(-\lambda_n t\right)\right] + \displaystyle\sum_{n=1}^{N} D_n\left[1-\exp\left(-\lambda_n\left(t-t_1\right)\right)\right]\end{array}\right.\end{aligned} \tag{5.3}$$

Then, the Prony series coefficients are determined by minimizing error between experimental measurements and predicted strains using Equation (5.3). Resulting coefficients of each mixture are listed in Table 5.1.

Table 5.1. Linear Viscoelastic Properties Represented by Prony Series Coefficients

Linear Viscoelastic Properties (in Prony Series Coefficients)			
n	λ_n (s^{-1})	D_n (MPa^{-1}) of Mixture 1 at 30°C	D_n (MPa^{-1}) of Mixture 2 at 40°C
1	10^2	6.70x10-4	9.07x10-4
2	10	8.91x10-5	3.18x10-4
3	1	5.17x10-4	6.29x10-4
4	10^{-1}	6.45x10-4	4.25x10-4
5	10^{-2}	9.47x10-4	1.03x10-3
6	10^{-3}	2.60x10-4	2.65x10-4
7	10^{-4}	2.73x10-4	2.73x10-4
8	10^{-5}	7.54x10-4	7.54x10-4

Once the Prony series coefficients have been obtained, the nonlinear viscoelastic parameters at higher stress levels can be determined. To do this, the recovered strains at high stress levels are used again with an assumption that the transient creep compliance is expressed in the form of a power law as follows, according to Lai and Bakker (1996):

$$\Delta D^{\psi^t} = D_c \psi^n \tag{5.4}$$

where D_c and n are material constants.

Substituting Equation (5.4) into Equations (5.1) and (5.2) gives:

$$\begin{aligned} \Delta\varepsilon(r) &= \varepsilon_c(t_1) - \varepsilon_r(t) \\ &= \alpha^* - \beta^* \left[(1 + a_\sigma \lambda)^n - (a_\sigma \lambda)^n \right] \end{aligned} \tag{5.5}$$

where

$$\alpha^* = g_0 D_0 \sigma + g_1 g_2 D_c \sigma \left(\frac{t_1}{a_\sigma} \right)^n \tag{5.6}$$

$$\beta^* = g_2 D_c \left(\frac{t_1}{a_\sigma} \right)^n \tag{5.7}$$

$$\lambda = \frac{t - t_1}{t_1} \tag{5.8}$$

Fitting Equation (5.5) to the recovered strains $\Delta\varepsilon_r$ can determine constants: n, α^*, β^*, and a_σ. It is also noted that n is almost stress-independent and can be obtained at a low stress level; therefore, the n value is fixed as a material constant, and the values of α^*, β^* and a_σ are obtained by repeating the fitting process. Next, g_2 is determined by minimizing errors between experimental data and Equation (5.7). Similarly g_0 and g_1 are determined from Equation (5.6). Table 5.2 presents the stress-dependent nonlinear viscoelastic parameters of the two asphalt mixtures tested at different temperatures.

Table 5.2. Stress-Dependent Nonlinear Viscoelastic Parameters of Each Mixture

Nonlinear Parameters	Temperature							
	Mixture 1 at 30°C			Mixture 2 at 40°C				
	Polynomial constants, *i*, in Equation (4.8)			Polynomial constants, *i*, in Equation (4.8)				
	1	2	3	1	2	3	4	5
g_0 (α_i)	0.05	0.77	-0.54	-0.12	0.43	-0.19	0.02	
g_1 (β_i)	0	0.01	-0.01	0	0	0	0	
g_2 (γ_i)	0.36	0.83	-0.71	-0.18	1.24	-2.08	1.2	-0.22
a_σ (δ_i)	-0.14	0.84	-0.83	0.31	-0.56	0.39	-0.09	

Values in Table 5.2 are represented graphically in Figure 5.2. As illustrated, all nonlinear viscoelastic parameters were fitted to polynomial functions so that each property can be represented as a function of stress levels. It is observed from the figure that parameter g_1 is not

significantly related to nonlinearity, whereas other parameters such as g_0 and g_2 are sensitively affected by stress levels. Both parameters generally increased as higher stresses were involved.

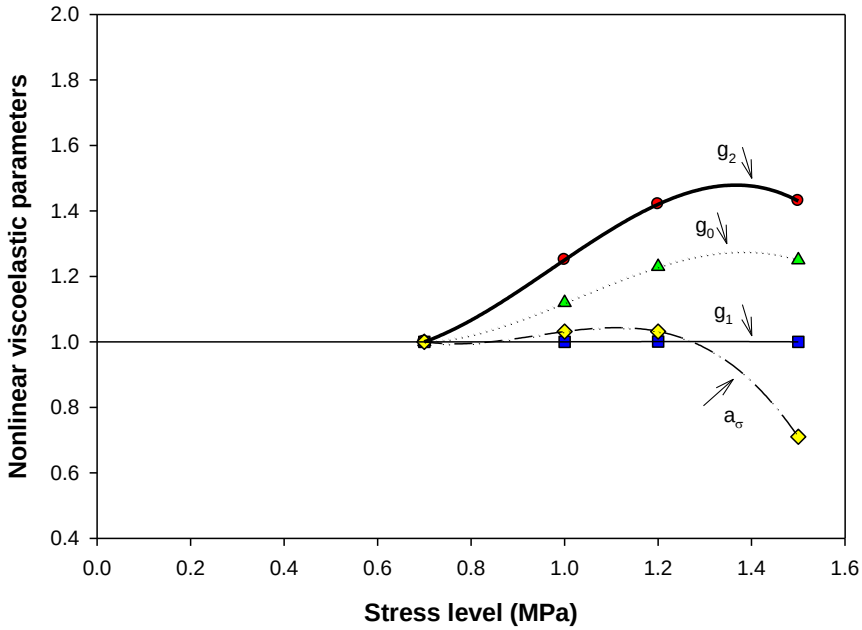

(a) Mixture 1 at 30°C

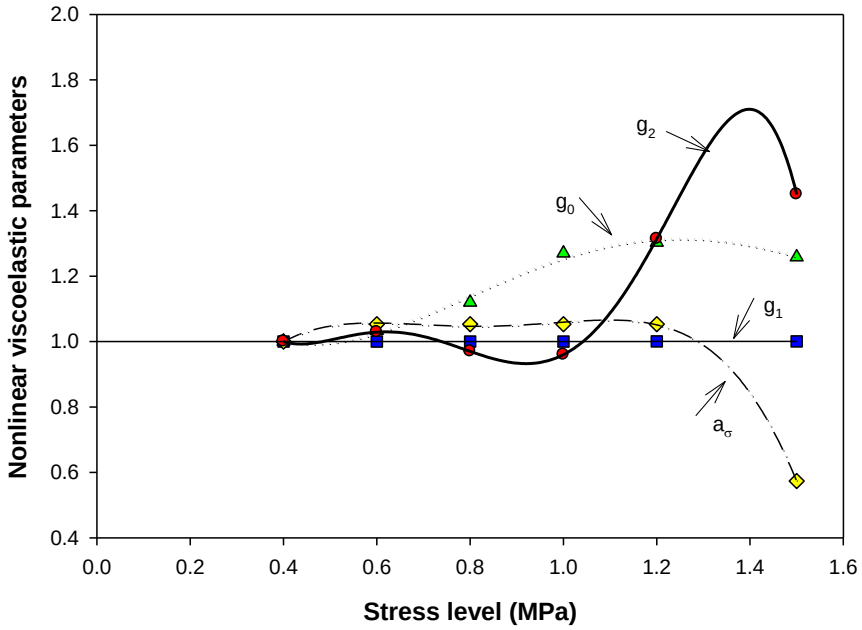

(b) Mixture 2 at 40°C

Figure 5.2. Stress-Dependent Nonlinear Viscoelastic Parameters of Each Mixture

5.2 MODEL VALIDATION

With the viscoelastic material properties (both linear and nonlinear) found, model validation was conducted by comparing FE model simulations to the creep-recovery test results. For simplicity, one element of a single creep-recovery test was simulated using the obtained material properties (i.e., Prony series coefficients and nonlinear viscoelastic parameters).

Figure 5.3 presents the comparisons of recovered strains between experimental results and numerical predictions. As shown in the figure, for the cases at threshold stress levels (700 kPa for Mixture 1 and 400 kPa for Mixture 2), results between testing and simulation are almost identical. As the level of stress becomes higher, slight discrepancies between testing and simulation are observed; however, overall simulation results show good agreement with the experimental data. This indicates that the developed UMAT is working properly and can be used to simulate the viscoelastic response of multilayered pavement structures in Chapter 6.

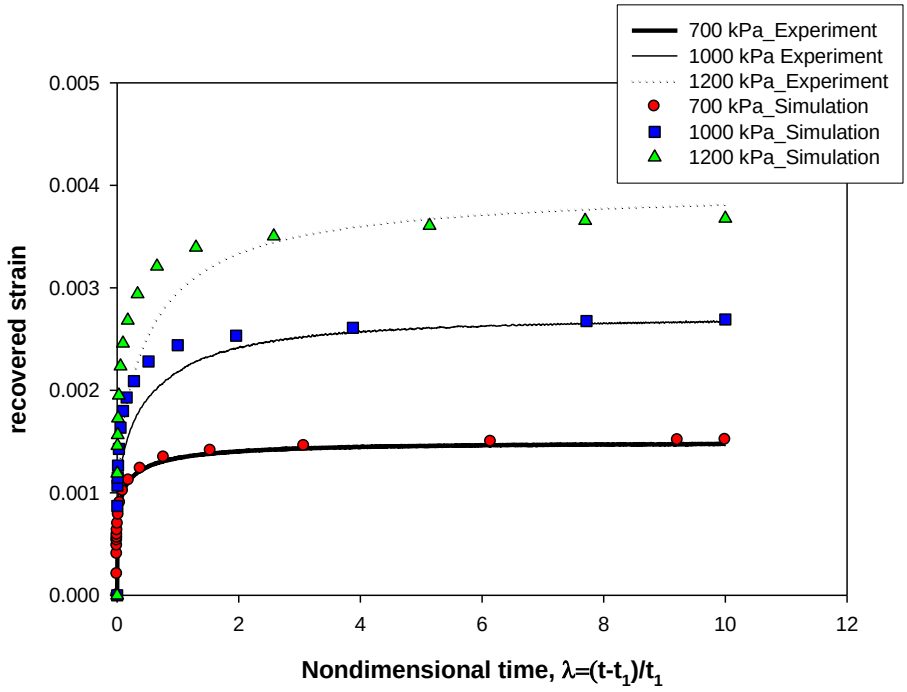

(a) Mixture 1 at 30°C

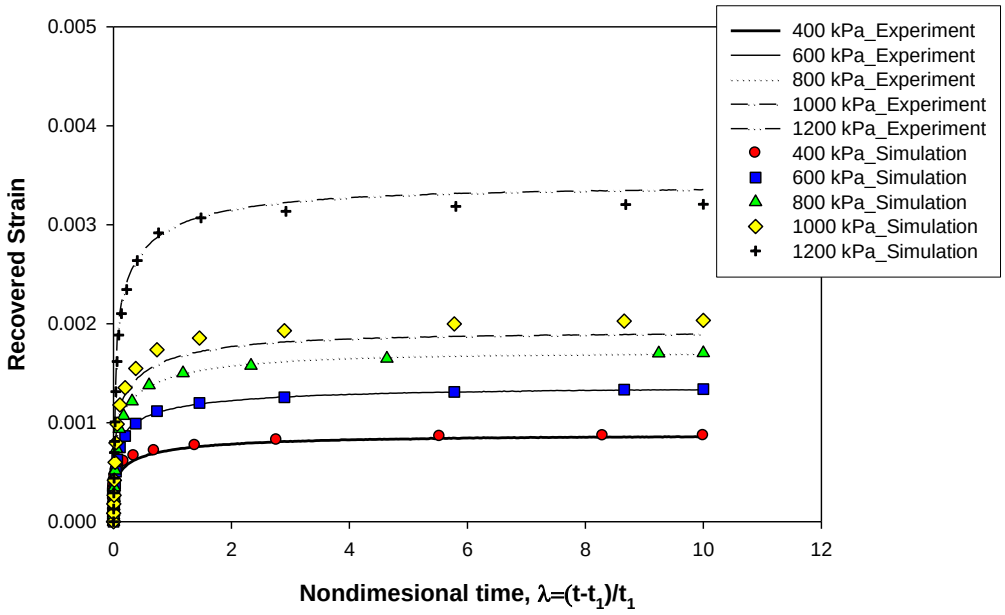

(b) Mixture 2 at 40°C

Figure 5.3. Comparison Plots between Model Predictions and Test Results

Once the viscoelastic strain is calculated using both the Prony series coefficients and the nonlinear viscoelastic parameters—which were found from only the recovered part of the strain in the creep-recovery test results—the total creep-recovery behavior can be used to capture any irrecoverable deformation of the mixtures by simply subtracting the viscoelastic (recoverable) strain from the total strain. For example, the decoupled viscoelastic strain and irrecoverable strain are shown in Figure 5.4 for Mixture 1 subjected to 1,000 kPa. As presented in the figure, a considerable amount of plastic (irrecoverable) strains are developed, which implies that a more proper form of the constitutive model eventually needs plastic and/or viscoplastic contribution in conjunction with the nonlinear viscoelastic characteristics to account for the overall mechanical behavior. Nevertheless, this study has not taken the plastic/viscoplastic responses into consideration. As mentioned previously, the primary target of this study is the examination of the

effects of nonlinear viscoelastic nature compared to simple linear viscoelasticity for predicting performance of asphalt pavements subjected to heavy truck loads.

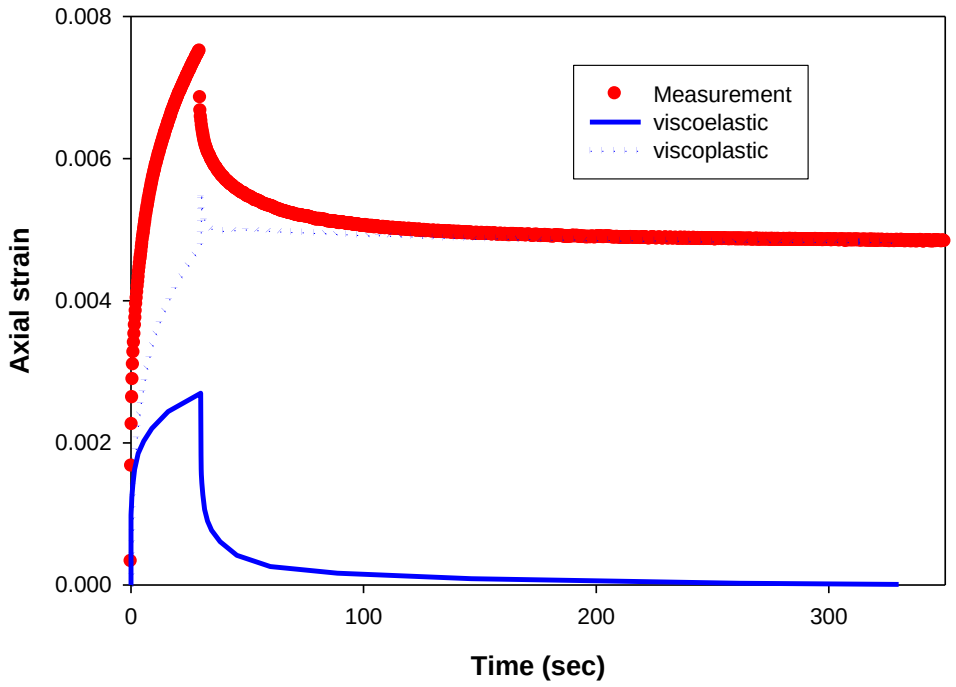

Figure 5.4. Strain Decomposition of the Creep-Recovery Test Results at 30^{o}C with 1,000 kPa

CHAPTER 6 FINITE ELEMENT ANALYSIS OF PAVEMENT

In this chapter, a standard asphalt pavement was modeled through the 3-D finite element method to investigate the mechanical performance behavior of the pavement when subjected to heavy truck loading. The 3-D finite element modeling was conducted by using a commercial package, ABAQUS Version 6.8 (2008), which is incorporated with the developed nonlinear viscoelastic UMAT. The model employed a time-marching computational simulation capable of predicting the spatial and temporal variations in stresses, strains, and displacements in the road. Simulation results comparing responses from linear viscoelasticity and from the use of nonlinear viscoelastic material characteristics are presented and discussed in this chapter.

6.1 PAVEMENT GEOMETRY AND BOUNDARY CONDITIONS

A typical flexible pavement structure was selected for simulations. Figure 6.1 illustrates a three-layered asphalt pavement structure (101.6-mm thick asphalt layer, 203.2-mm thick base, and 1270-mm subgrade) and its 3-D finite element mesh. Only a quarter of the whole domain with a single axle loading in dual-tire is modeled due to its symmetry. The right hand side of the vertical edge is fixed in the horizontal direction; the bottom of the mesh is fixed in the vertical direction representing a bed rock. In order to alleviate computational expense, infinite elements (CIN3D8 in ABAQUS) were used at the boundaries far from the loading zone.

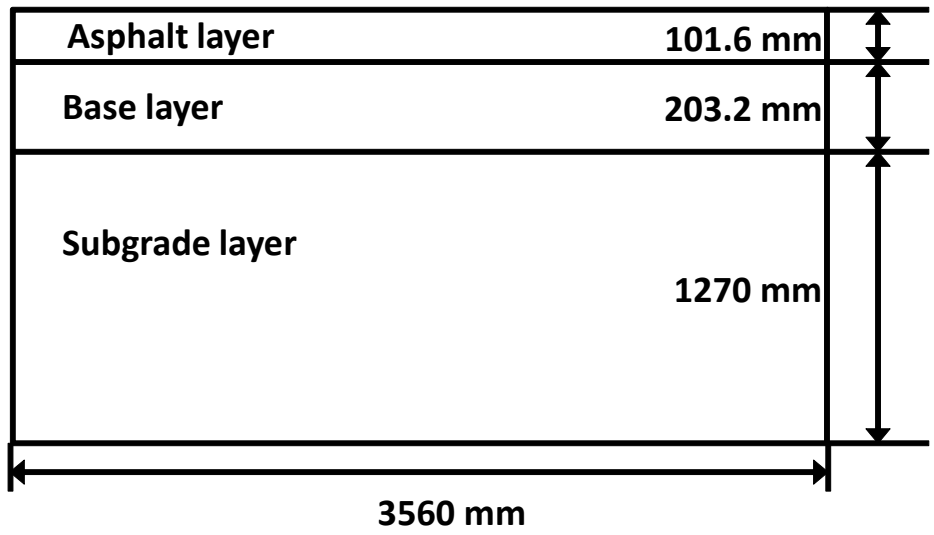

(a) Three-Layered Asphalt Pavement Structure to be Modeled

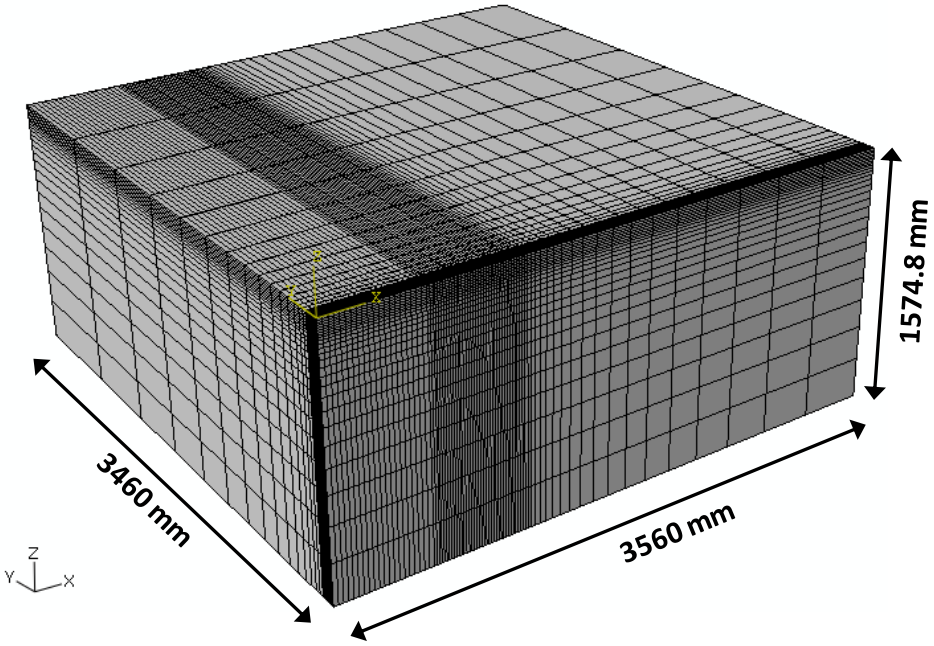

(b) Three-Dimensional Finite Element Mesh

Figure 6.1. A Pavement Geometry Selected for Finite Element Modeling

Figure 6.2 illustrates the tire loading configuration used in this study. Traditionally, either circular or rectangular distribution of contact pressure has been applied to model tire loading for simplicity, although neither represents real tire footprints. Since this study attempts to model pavements as realistically as possible based on the 3-D finite element mesh, the actual tire footprints can be simulated. Figures 6.2(a) present the real footprint of dual tire with inflation pressure of 720 kPa and axial load of 35.5 kN (Yoo 2007). For FE simulation, the tire footprints were applied to the pavement surface with contact pressure shown in Figure 6.2(b).

(a) Tire Footprints

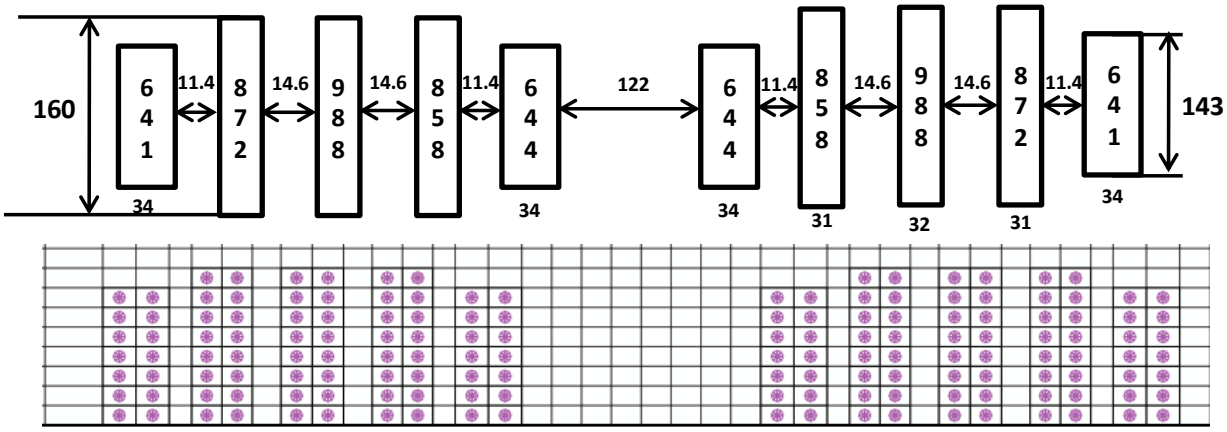

(b) Tire Pressure Distributions Applied to the Mesh

Figure 6.2. Tire Loading Configuration

Figure 6.3 illustrates the loading configuration of the Class 9 truck used in this study (Soares et al. 2008). Although the truck loading consists of a front steer axle and two tandem axles with dual tires, to reduce computational time in the analysis only the two tandem axles with dual tires were selected through use of the trapezoidal loading sequence shown in Figure 6.3. A 15.4 m Class 9 truck trailer traveling at 80 km/h takes 0.692 seconds to pass over a fixed point on the pavement. Therefore, the first truck passes the fixed point for 0.692 seconds and after 30 seconds a second truck passes through the same point. The passage of a total of 50 trucks was simulated.

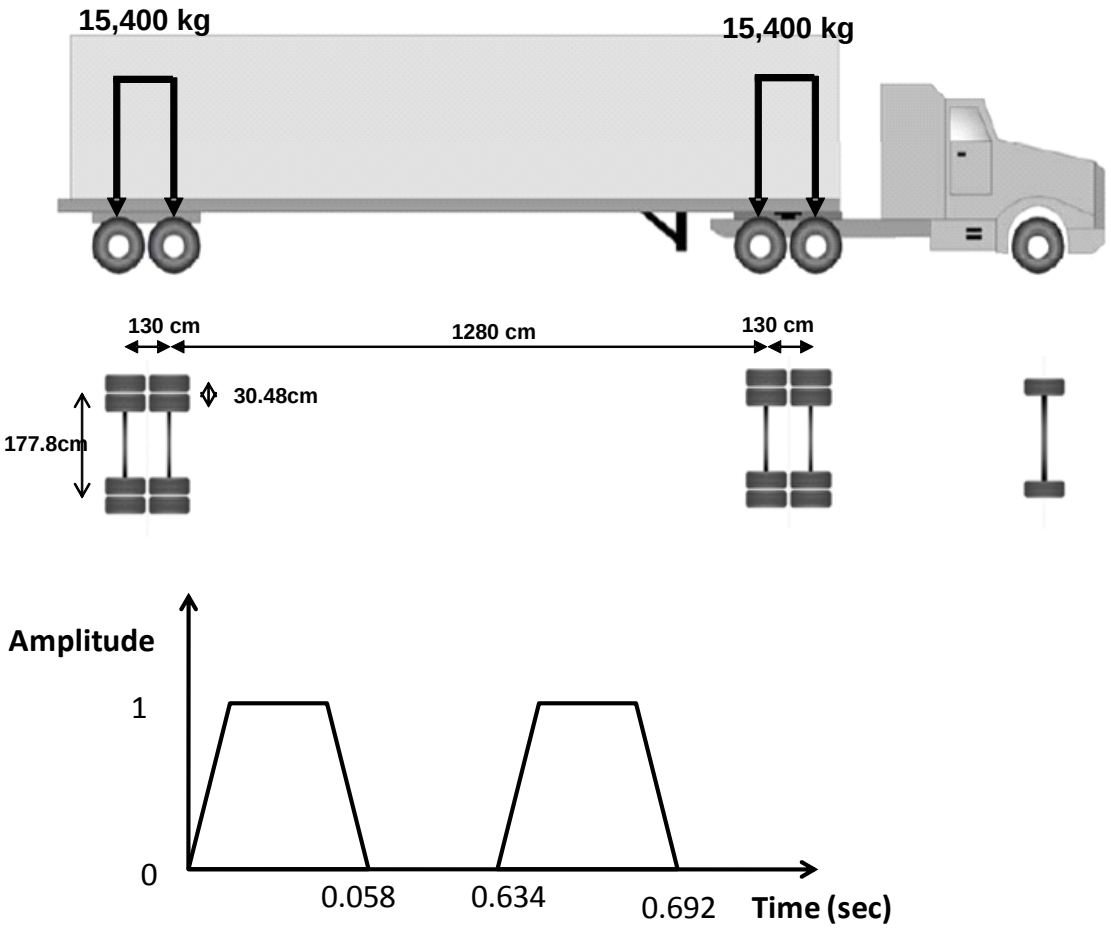

Figure 6.3. Truck Loading Configuration (Class 9) Used in This Study

6.2 LAYER PROPERTIES

Table 6.1 presents material properties of individual layers. The underlying layers (i.e., base and subgrade) were modeled as isotropic linear elastic, while viscoelastic response was considered to describe the behavior of the asphalt concrete surface layer. The surface layer can dissipate energy due to its viscoelastic nature, which results in permanent deformation (rutting) of the layer. Different performance responses between the linear and nonlinear viscoelastic approaches can be compared, and the resulting significance of the nonlinear viscoelastic nature of asphalt mixtures can be observed. For this analysis, viscoelastic properties of Mixture 1 were used as presented in the table.

Table 6.1. Material Properties of Each Layer

Linear Elastic Material Properties			
Layer	E (MPa)		υ
Base	350		0.35
Subgrade	138.64		
Linear Viscoelastic Properties of Mixture 1			
	n	λ_n (s^{-1})	D_n (MPa^{-1})
Asphalt Concrete	1	10^{2}	6.70×10^{-4}
	2	10	8.91×10^{-5}
	3	1	5.17×10^{-4}
	4	10^{-1}	6.45×10^{-4}
	5	10^{-2}	9.47×10^{-4}
	6	10^{-3}	2.60×10^{-4}
	7	10^{-4}	2.73×10^{-4}
	8	10^{-5}	7.54×10^{-4}
Nonlinear Viscoelastic Parameters of Mixture 1			
	Polynomial constants, i, in Equation (3.8)		
	Parameters	1	2	3
Asphalt Concrete	$g_0(\alpha_i)$	0.05	0.77	-0.54
	$g_1(\beta_i)$	0	0.01	-0.01
	$g_2(\gamma_i)$	0.36	0.83	-0.71
	$a_\sigma(\delta_i)$	-0.14	0.84	-0.83

6.3 SIMULATION RESULTS

This subsection presents simulation results and differences in pavement responses between the two attempts, which modeled the asphalt concrete layer using either linear viscoelastic properties or nonlinear viscoelastic parameters. Among many mechanical responses, the vertical displacement from the surface and the horizontal strain at the bottom of asphalt layer are examined with the 50 cycles of truck loading (as was described earlier). This is because the vertical displacement and the horizontal strain are strongly related to two primary pavement distresses: rutting and fatigue cracking.

6.3.1 Permanent Deformation (Rut Depth)

Figure 6.4 compares permanent deformation (rut depth) accumulated from each truck loading up to the 50 cycles. It clearly shows the increasing difference in the rut depth between the two models as the number of loading cycles increases. This is because the stress-dependent nonlinear viscoelastic parameters increase as stress level increases, as demonstrated in Chapter 4. At the end of the 50 cycle simulation, the total rut depth predicted from the nonlinear viscoelastic case was around 500% more than the total rut depth predicted through use of the linear viscoelastic model. This clearly indicates that performance-based design of pavement structures should be based on a proper characterization of materials that is as realistic as possible.

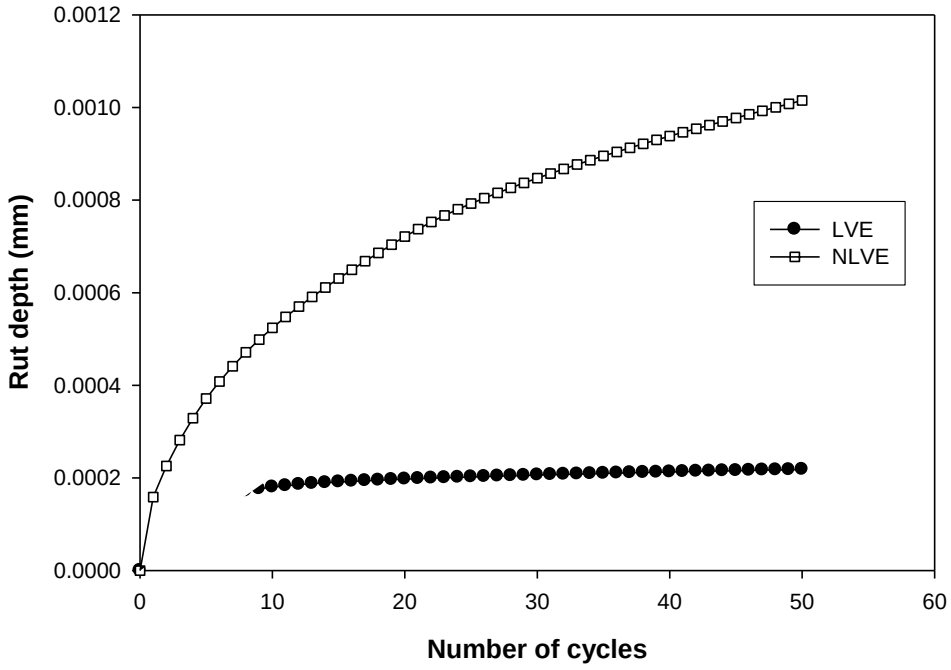

Figure 6.4. Comparison of Permanent Deformation up to 50 Loading Cycles: LVE vs. NLVE

Figure 6.5 shows vertical displacement plots across the transverse section at two different loading cycles: 1 and 50. Similar to the results illustrated in Figure 6.4, it shows that increasing loading cycles develop greater difference to the permanent deformation between the two approaches. It is also observed that both approaches can predict the apparent heave between the two wheels; however the heaving located at the sides of the wheels was only visible for the nonlinear viscoelastic case. This result demonstrates, at least in a qualitative manner, that the modeling based on the nonlinear viscoelastic material characteristics is better capable of representing this often observed physical phenomenon than is the linear viscoelastic modeling.

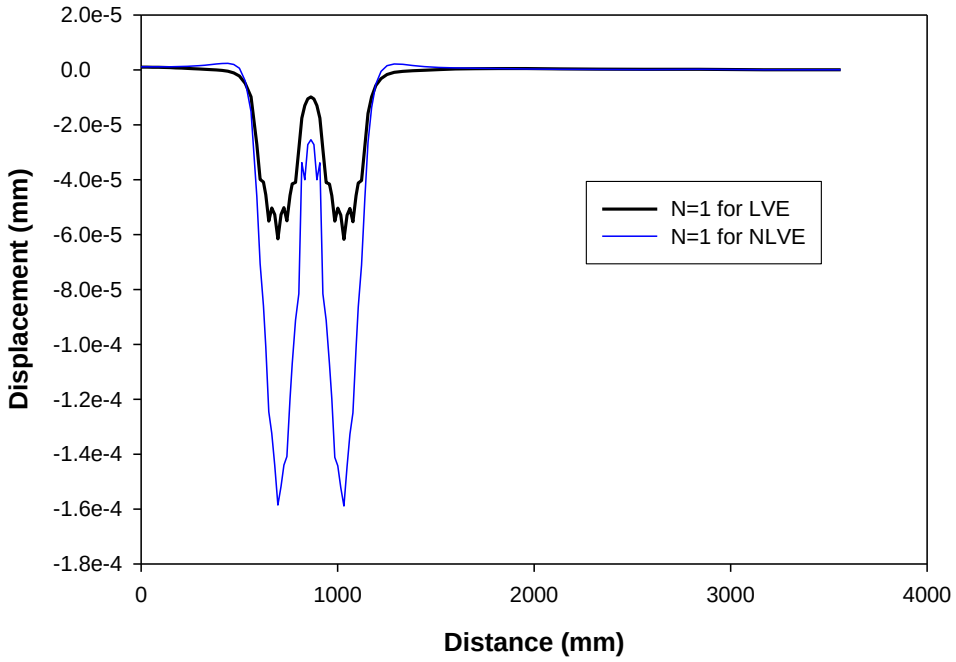

(a) 1st Cycle

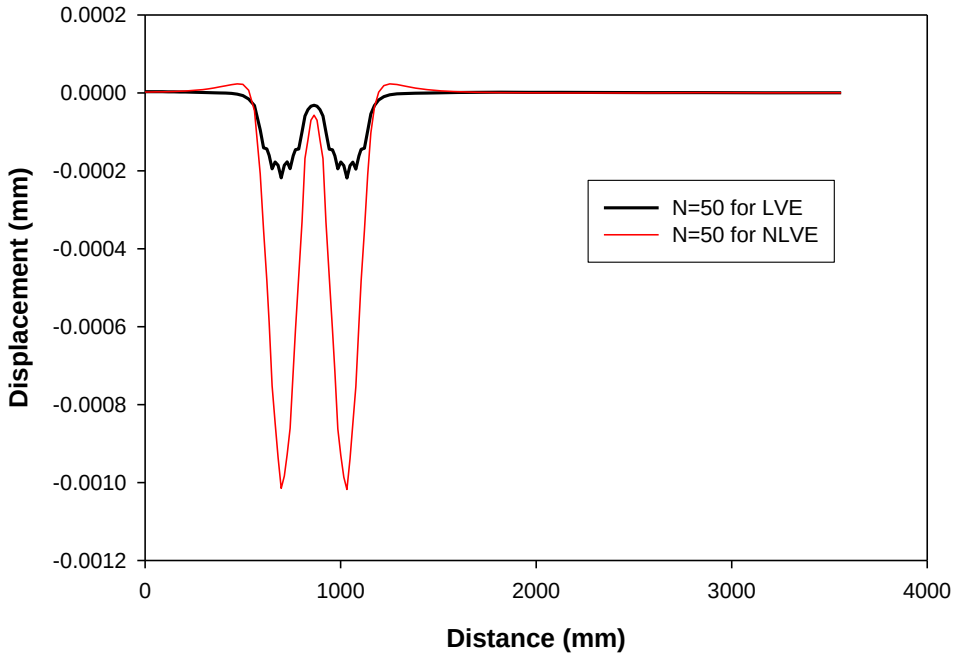

(b) 50th Cycle

Figure 6.5. Comparison of Vertical Displacement Plots across the Transverse Section

Figure 6.6 shows contour plots of vertical displacement distributions in the asphalt layer for different numbers of loading cycles (i.e., 10, 30 and 50 cycles) obtained from the two modeling approaches. Contour plots in the left side are the results from the linear viscoelastic simulation, while the plots on the right were obtained with consideration of the nonlinear viscoelasticity of asphalt layer. These plots clearly show that vertical displacement from the nonlinear viscoelastic model propagates much more quickly to the bottom of the asphalt layer than does vertical displacement from the linear viscoelastic model when the number of loading cycles is increased.

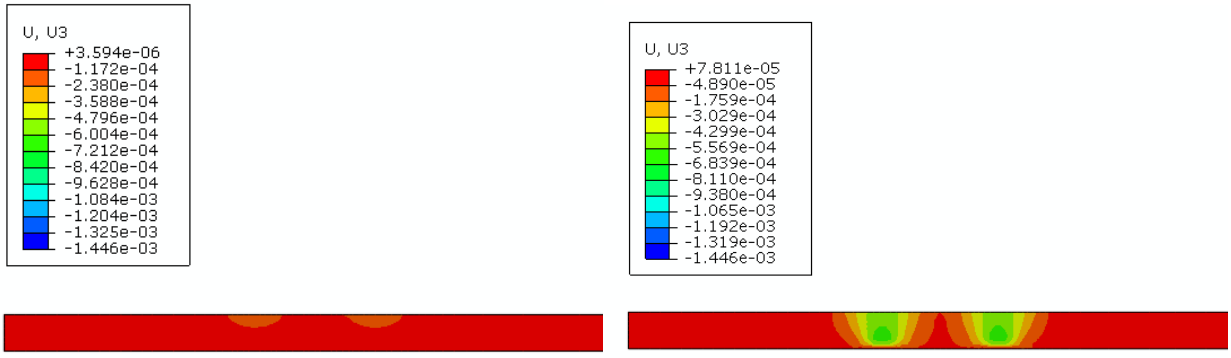

(a) 10th Cycle

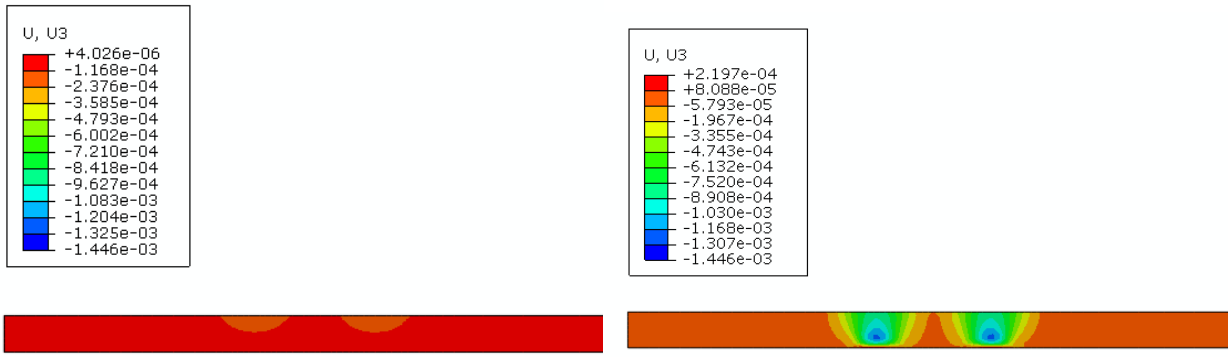

(b) 30th Cycle

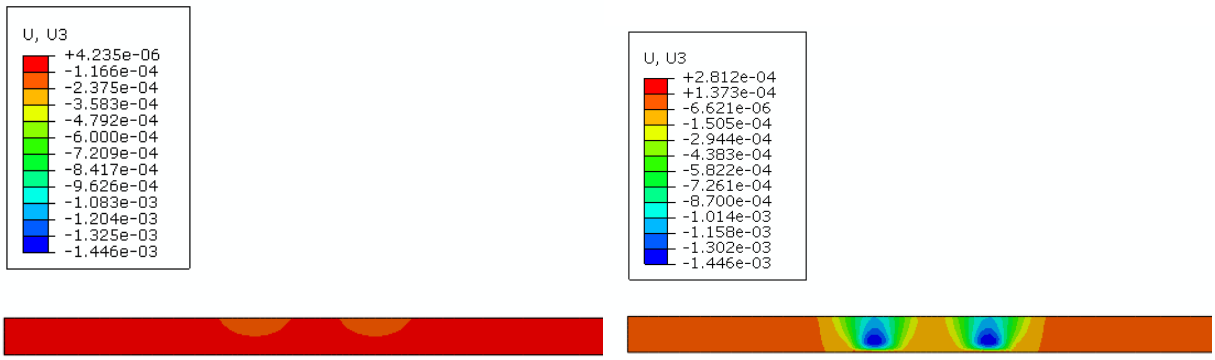

(c) 50th Cycle

Figure 6.6. Contour Plots of Vertical Displacement Distributions: LVE vs. NLVE

6.3.2 Horizontal Strain

Figure 6.7 compares maximum horizontal strains (in tension) at the bottom of the asphalt layer for up to 50 truck loading cycles. Interestingly, the horizontal strains appeared to be constant with the linear viscoelastic model of the asphalt layer. In the case of the nonlinear viscoelastic asphalt layer, the horizontal strains increased as the loading cycle increased, which is a trend similar to that shown for the vertical displacement presented in Figure 6.4. Accumulation of horizontal tensile strains at the bottom of the asphalt layer is directly associated with the phenomenon of cracking in asphalt pavements. Therefore, the observed difference between the two approaches is considered significant and should be addressed in the process of performance-based pavement design. Furthermore, this finding implies that proper and more realistic characterization of materials behavior is necessary.

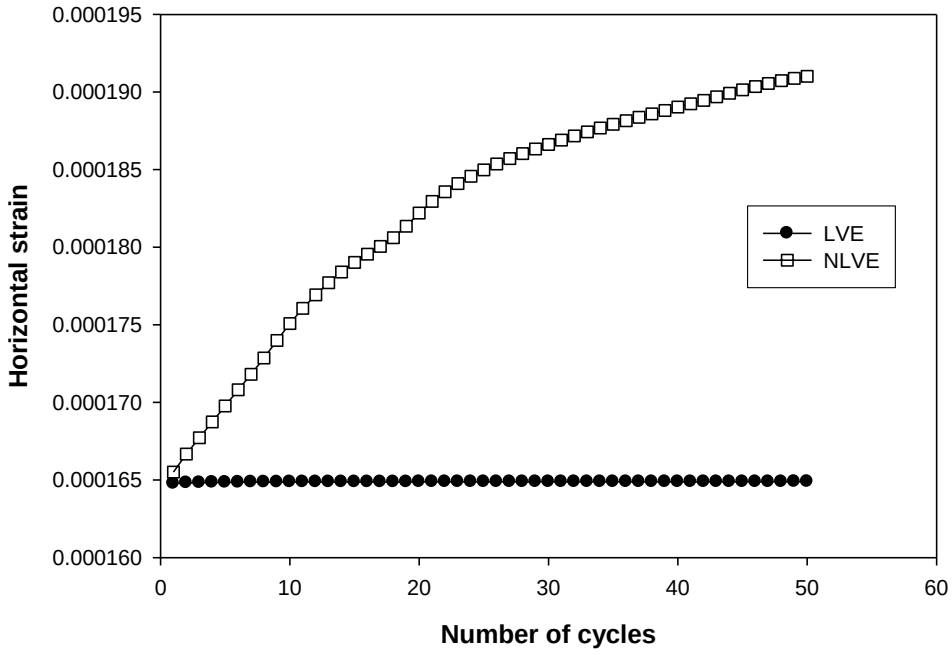

Figure 6.7. Comparison of Horizontal Strain up to 50 Loading Cycles: LVE vs. NLVE

Figure 6.8 shows horizontal strain profiles along the transverse section at two different loading cycles: 1 and 50. Note that the sign convention adopted herein is positive for tension. As shown in the figure, the maximum tensile strains take place below the tire, and compressive strains develop between the tires. At the first loading cycle the developed horizontal strains between the two models are almost identical. As the loading cycle increased, the nonlinear viscoelastic model predicted greater maximum tensile strains, whereas the linear viscoelastic model did not show any significant changes from the initial stage. Strain profiles at the 50th loading cycle clearly demonstrate the difference in responses between the two approaches as specified with the arrows in Figure 6.8(b).

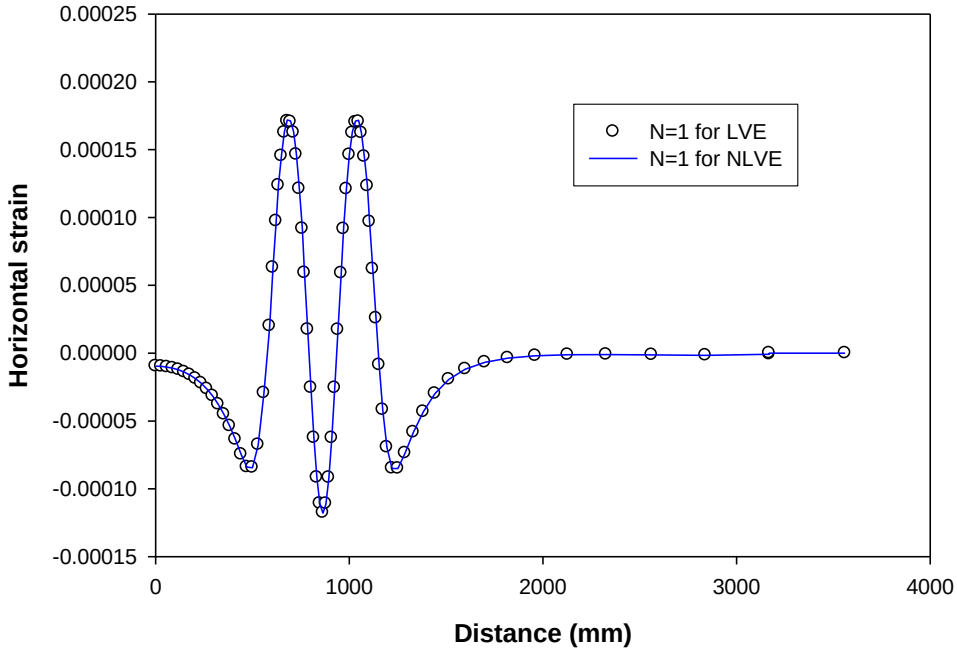

(a) 1st Cycle

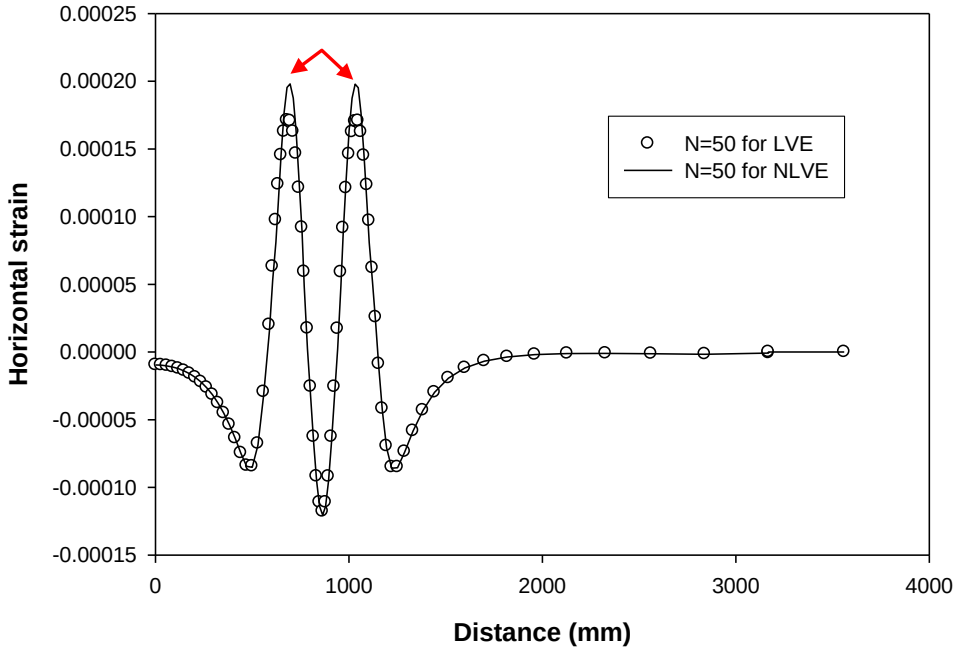

(b) 50th Cycle

Figure 6.8. Comparison of Horizontal Strain Plots across the Transverse Section

Finally, Figure 6.9 illustrates contour plots of horizontal strains obtained from the two modeling approaches in the asphalt layer for different loading stages (i.e., 10, 30 and 50 cycles). Since the magnitude of strain differences between the two models is not great, the contours at each loading cycle are not significantly distinctive. However, as shown in the contour legend of each loading cycle, the maximum horizontal strain observed from the nonlinear viscoelastic model is greater and kept increasing with increased loading cycles, while the maximum and minimum horizontal strains resulting from the linear viscoelastic case did not vary at different loading cycles.

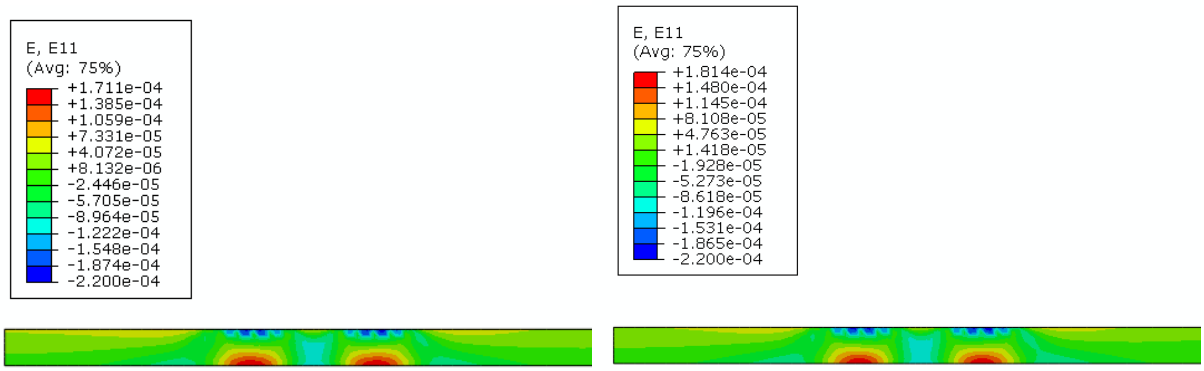

(a) 10th Cycle

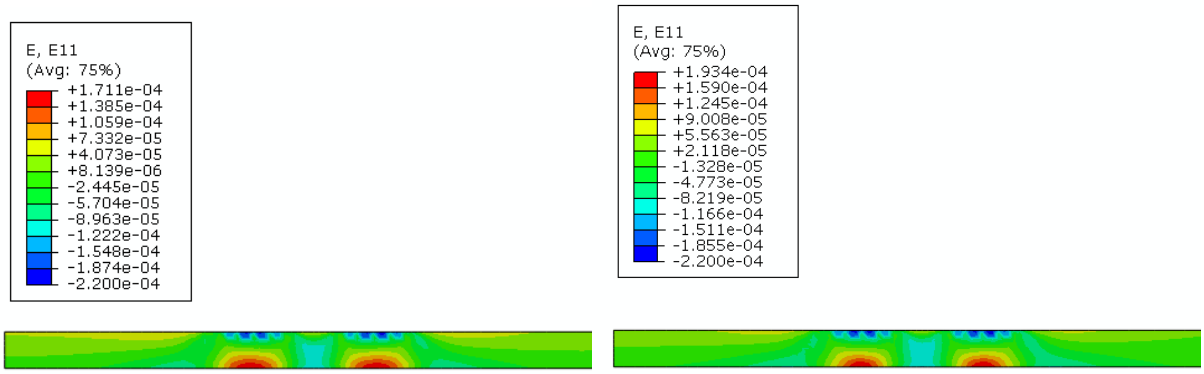

(b) 30th Cycle

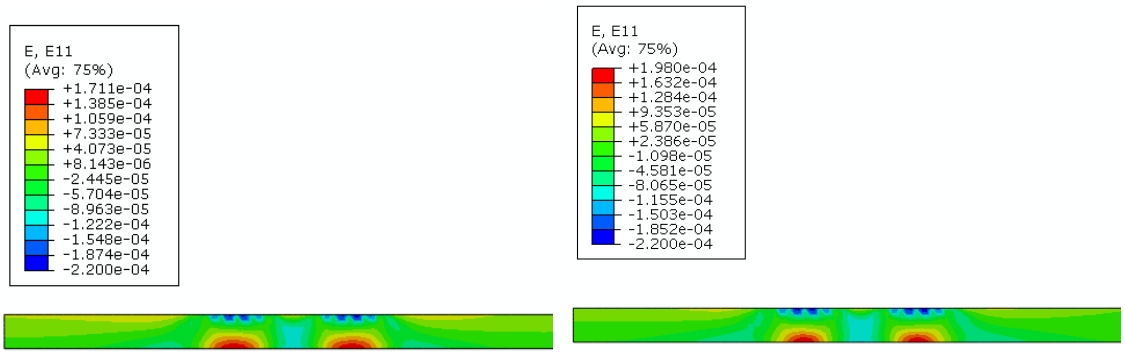

(c) 50th Cycle

Figure 6.9. Contour Plots of Horizontal Strain Distributions: LVE vs. NLVE

CHAPTER 7 SUMMARY AND CONCLUSIONS

As a continuation to previous research, Kim et al. (2009), we have sought a more advanced constitutive model for asphalt mixtures to more accurately predict pavement responses. To this end, Schapery's nonlinear viscoelastic constitutive model was implemented into the commercial FE software ABAQUS via user defined subroutine (UMAT) to analyze asphalt pavements subjected to heavy truck loads. Then, extensive creep-recovery tests were conducted at various stress levels and at two temperatures (30^{o}C and 40^{o}C) to obtain the stress- and temperature-dependent viscoelastic material properties of hot mix asphalt (HMA) mixtures. With the viscoelastic material properties characterized, a typical pavement structure was modeled with consideration of the effect of material nonlinearity with a realistic tire loading configuration.

Detailed investigations of the pavement responses resulting from different constitutive relations (i.e., linear viscoelastic and nonlinear viscoelastic) provided interesting observations and findings that could be used to better understand the effects of truck loading on pavement damage, and consequently to further advance current pavement-analysis design methods. The following bullets summarize conclusions that can be drawn.

- Schapery's nonlinear viscoelastic model was well implemented into the ABAQUS via a user material subroutine UMAT. Two example problems presented in this study verified the model and its numerical implementation.
- Creep-recovery tests at varying stress levels and different temperatures were conducted with different asphalt concrete mixtures to identify viscoelastic mixture characteristics. As expected, test results clearly demonstrated stress level-, temperature- and material-dependent mixture characteristics.

- With the creep-recovery test results, a series of processes was applied to identify linear and nonlinear viscoelastic properties. Linear viscoelastic properties were characterized by the Prony series based on the generalized Maxwell model, and nonlinear viscoelastic parameters were successfully fitted to polynomial functions, which enables individual nonlinear viscoelastic properties to be represented as a continuous function of stress levels.
- The viscoelastic material properties could be validated by comparing single-element FE model simulations to the creep-recovery test results for the recoverable strains. However, when the viscoelastic characteristics were applied to the prediction of total creep-recovery strain behavior in cases where unrecoverable strains also exist, a considerable amount of plastic strains developed, implying the necessity of plastic and/or viscoplastic material modeling as well as the nonlinear viscoelastic model to account for overall material behavior.
- Three-dimensional finite element simulations of a pavement structure presented significant differences between the linear viscoelastic approach and the nonlinear viscoelastic modeling in the prediction of pavement performance (e.g., rutting and fatigue cracking). It was observed that linear viscoelastic analysis of asphalt pavements underestimates mechanistic responses. The differences between the two approaches are considered significant and should be addressed in the process of performance-based pavement design. This further implies the importance of proper and more realistic characterization of materials.
- Although the nonlinear viscoelastic model attempted in this study provided better insights into the performance of asphalt pavements, additional constitutive models, such as plastic and/or viscoplastic modeling, and inclusion of damage due to discrete fracture (i.e., cracks) remain topics for future work.

REFERENCES

ABAQUS. 2008. version 6.8. Hibbt, Karlsson, and Sorenson, Inc.: Pawtucket, Rhode Island.

Airey, G., B. Rahimzadeh, and A. C. Collop. 2004. "Linear Rheological Behavior of Bituminous Paving Material." *Journal of Materials in Civil Engineering* 16: 212–220.

Al-Qablan, H., A. Saleeb, and R. Y. Liang. 2006. "Mechanistic Modeling of Rutting in Asphalt Pavement Analyzer (APA) Tests." *Pavement Mechanics and Performance* GSP 154: 63-74.

Al-Qadi, I. L., A. Loulizi, I. Janajreh, and T. E. Freeman. 2002. "Pavement Response to Dual and New Wide Base Tires at the Same Tire Pressure." *Transportation Research Record* 1806: 38-47.

Al-Qadi, I. L., M. A. Elseifi, and P. J. Yoo. 2004. "In-situ Validation of Mechanistic Pavement Finite Element Modeling." Proceedings, 2nd Int. Conference on Accelerated Pavement Testing, Minneapolis.

Al-Qadi, I. L., P. J. Yoo, and M. A. Elseifi. 2005. "Characterization of Pavement Damage Due to Different Tire Configurations." *Journal of the Association of Asphalt Paving Technologists* 74: 921-962.

Burmister, D. M. 1943. "The Theory of Stresses and Displacements in Layered Systems and Application to the Design of Airport Runways." *Highway Research Board* 23: 126-144.

Blab, R., and J. T. Harvey. 2002. "Modeling Measured 3D Tire Contact Stresses in a Viscoelastic FE Pavement Model." *International Journal of Geomechanics* 2.3: 271-290.

Cho, Y. H., B. F. McCullough, and J. Weissmann. 1996. "Considerations on Finite-Element Method Application in Pavement Structural Analysis." *Transportation Research Record* 1539: 96-101.

Collop, A. C., A. Scarpas, Cor Kasbergen, and A. Bondt. 2003. "Development and Finite Element Implementation of Stress-Dependent Elastoviscoplastic Constitutive Model with Damage for Asphalt." *Transportation Research Record* 1832: 96-104.

Elseifi, M. A., and I. L. Al-Qadi. 2006. "Modeling of Strain Energy Absorbers for Rehabilitated Cracked Flexible Pavements." *Journal of Transportation Engineering* 131.9: 653-661.

Elseifi, M. A., I. L. Al-Qadi, and P. J. Yoo. 2006."Viscoelastic Modeling and Field Validation of Flexible Pavements." *Journal of Engineering Mechanics* 132.2: 172-178.

"Freight Transportation Profile–Nebraska Freight Analysis Framework." 2002. *FHWA Freight News*. Office of Freight Management and Operations, US-DOT.

Haji-Ali, R., and A. Muliana. 2004. "Numerical Finite Element Formulation of the Schapery Non-Linear Viscoelastic Material Model." *International Journal for Numerical Methods in Engineering* 59: 25-45.

Helwany, S., J. Dyer, and J. Leidy. 1998. "Finite-Element Analyses of Flexible Pavements." *Journal of Transportation Engineering* 124.5: 491-499.

Huang, C. W., R. K. Abu Al-Rub, E. A. Masad, and D. N. Little. 2011. "Three-Dimensional Simulations of Asphalt Pavement Permanent Deformation Using a Nonlinear Viscoelastic and Viscoplastic Model." *Journal of Materials in Civil Engineering* 23.1: 56-68.

Kim, D., R. Salgado, and A. G. Altschaeffl. 2005. "Effects of Supersingle Tire Loadings on Pavements." *Journal of Transportation Engineering* 131.10: 732-743.

Kim, J., R. Roque, and T. Byron. 2009. "Viscoelastic Analysis of Flexible Pavements and its Effects on Top-Down Cracking." *Journal of Materials in Civil Engineering* 27.7: 324-332.

Kim, J., T. Byron, G. A. Sholar, and S. Kim. 2008. "Comparison of a Three-Dimensional Visco-Elastic Modeling and Field Validation of Flexible Pavements." Presented at the TRB Annual Meeting (CD-ROM), Washington D.C.

Kim, Y. R., D. H. Allen, and G. D. Seidel. 2006. "Damage-Induced Modeling of Elastic-Viscoelastic Randomly Oriented Particulate Composites." *Journal of Engineering Materials and Technology* 126: 18-27.

Kim, Y. R., H. Ban, and S. Im. 2010. "Impact of Truck Loading on Design and Analysis of Asphaltic Pavement Structures." MATC Final Report No. 223, Lincoln, Nebraska.

Lai, J., and A. Bakker. 1996. "3-D Schapery Representation for Non-Linear Viscoelasticity and Finite Element Implementation." *Computational Mechanics* 18: 182-191.

Masad, E., and N. Somadevan. 2002. "Microstructural Finite-Element Analysis of Influence of Localized Strain Distribution of Asphalt Mix Properties." *Journal of Engineering Mechanics* 128: 1105–1114.

Mun, S., M. Guddati, and Y. R. Kim. 2004. "Fatigue Cracking Mechanisms in Asphalt Pavements with Viscoelastic Continuum Damage Finite-Element Program." *Transportation Research Record* 1896: 96-106.

Myers, L., R. Roque, and B. Birgisson. 2001. "Use of Two-Dimensional Finite Element Analysis to Represent Bending Response of Asphalt Pavement Structures." *International Journal of Pavement Engineering* 2: 201-214.

National Cooperative Highway Research Program (NCHRP) Project 1-37A. 2004. "Guide for Mechanistic-Empirical Design of New and Rehabilitated Pavement Structures." Final Report.

Schapery, R. A. 1969. "On the Characterization of Nonlinear Viscoelastic Materials." *Polymer*

Engineering and Science 9: 295-310.

Soares, R. F., D. H. Allen, Y. Kim, C. Berthelot, J. B. Soares, and M. E. Rentschler. 2008. "A Computational Model for Predicting the Effect of Tire Configuration on Asphaltic Pavement Life." *International Journal on Road Materials and Pavement Design* 9.2: 271-289.

Wang, J. 2001. "Three-dimensional Finite Element Analysis of Flexible Pavements." M.S. Thesis, University of Maine.

Yoo, P. J., I. L. Al-Qadi, M. A. Elseifi, and I. Janajreh. 2006. "Flexible Pavement Responses to Different Loading Amplitudes Considering Layer Interface Condition and Lateral Shear Forces." *International Journal of Pavement Engineering* 7.1: 73-86

Yoo, P. J. 2007. "Flexible Pavement Dynamic Responses Analysis and Validation for Various Tire Configurations." Ph.D. Diss., University of Illinois at Urbana-Champaign.

Zhao, Y. 2002. "Permanent Deformation Characterization of Asphalt Concrete Using a Viscoelasticplastic Model." Ph.D. Diss., North Carolina State Univ.